People's Democratic Republic of Algeria

Ministry of Higher Education and Scientific Research

University M'HAMED BOUGARA – Boumerdes

Institute of Electrical and Electronic Engineering

Department of Electronics

Final Year Project Report Presented in Partial Fulfilment of the Requirements for the Degree of

MASTER

In **Telecommunication**

Option: **Telecommunications**

Title:

Contribution to the design of MIMO Ultra-Wide Band Monopole antenna

Presented by:

- BACHA Amina
- BENSAYAH Hiba

Supervisor:

Pr. A. AZRAR

Registration Number:……...../2021

Abstract

This work presents the design UWB MIMO antennas with reduced Mutual coupling. The work is started by the design and analysis of a rectangular monopole that operates as UWB structure. The Bandwidth is further enlarged by introducing the concavities in the non-radiating edges of the rectangular monopole. The obtained structure conserves the far field characteristics with an increase in the bandwidth.

The design is extended to two rectangular monopoles for MIMO applications. The observed mutual coupling is reduced by embedding a rectangular metallic isolator between the patches. A further decrease in the mutual coupling is carried out by replacing the rectangular monopoles by concaved monopoles. Eventhough isolation between the elements of the MIMO structures is reached; the main beam radiation direction is deflected opposite to the isolator wall in the E-plane with high level cross-polar component in the H-plane.

To confirm the near zone results, the concaved MIMO structure fabricated on the FR4 dielectric substrate. The measurements of the input reflection and the transmission coefficients present agreement with simulations within the limits of measurement conditions.

DEDICATION

To

My Father

who were a great mentor and supporting and encouraging me to believe in myself.

My Mother

A strong and gentle soul who taught me to trust in Allah, supporting me throughout the years, teaching me and sharing in my triumphs and my tears.

My Sister Soumia & My Brother Abd Elmouaine

You are my supporters, my happiness, my audience, my biggest fans, my best friends…

My Cousin Annes

You are the happiness and the joy in our family and the most beautiful thing that happened.

My Second Family

All my friends who have never left my side and supported me throughout 5 years specially Zahra, Lydia and Manel.

My Partner Hiba

Thank you for always being there, for making me smile and for constantly supporting me in all my states.

Without forgetting a special person Abdelmalek who was always here for me and pushed me to work hard, and been a source of encouragement and inspiration.

Amina

DEDICATION

To

My Mother & My Father

A special feeling of gratitude to my parents who always picked me up on time and encouraged me to go on every adventure, especially this one.

Thank you!

My Sisters & My Brothers

You are my beginning, you are my end, you are all around me when the world turns away, you are my sunshine on a cloudy day, I can always lean on you, you are everything.

Thank you!

My Nieces & My nephews

You are my happiness and the most beautiful thing that happened to me to become your aunt.

I love you!

My Second Father

Without forgetting a special person my uncle CHARIF who encouraged me and helped me to overcome many difficulties.

Thank you!

My Friends

You are my second family, you stood by me, supported me, and made me happy in the most difficult times. Especially Asma, Tassadit, Amira, Kenza and Islam.

Thank you for giving me the best memories!

My Partner Amina

Without you, I would not have accomplished this work.

Thank you for your hard work and your patience with me.

Thank you for everything!

Hiba

Acknowledgement

Primarily, we are very grateful to ALLAH for giving us the key and opportunity to accomplish our Final Year Project.

In particular, a special greeting goes to Pr. Arab AZRAR, who was our supervisor, for his patience and his support on the way, and for his useful comments, remarks, and engagement through the completion of this master thesis. You have been the ideal project supervisor.

We would like to express our sincere gratitude to Mrs. MOUHOUCH and Mrs. DJAFRI for their guidance, support and for gracefully providing us with required facilities for simulations, fabrication and the experimentation processes of our project

We wish to thank lecturers, staff and technicians, for their cooperation, indirect or direct contribution in finishing our project. Our sincere appreciation also to all our friends who have involved and helped us in this project especially HAMRIOUI Fatma Zohra and AISSAOUI Abderrahman.

Most importantly, we wish our gratitude to our parents and all family members for their support, encouragement, under-standing, sacrifice and love.

Table of Contents

Table of Contents

List of tables

List of figures

General Introduction

Antenna is usually defined as a metallic device (as a rod or wire) for radiating and receiving radio waves. Antennas play a very important role in the field of wireless communications, as it is the transitional structure between free-space and a guiding device. In other word, antenna is a transducer that converts electric power into electromagnetic waves and transmits or receives the electromagnetic waves using a conductor [1].

There are many forms of antennas each of which are characterized by specific features and desirable for specific use. In the recent years of development in communication systems, a need for the development of lightweight, compact and cost-effective antennas that are capable of maintaining high performance over a wide spectrum of frequencies. This technological trend has focused much effort into the design of a microstrip patch antenna [2].

In this project, the main objective is to design MIMO antenna with reduced coupling operating in an UWB system. At the beginning, generalities about microstrip antennas and MIMO – Ultra Wide Band antennas are presented. Then, a single rectangular monopole antenna is designed and the effect of introducing a concavity is studied. At the end, the effect of concavity and isolator on rectangular MIMO antenna is investigated. The simulated results are confirmed using measurement of the realized structure.

CHAPTER 1

Generalities about Microstrip antennas and MIMO – Ultra Wide Band antennas

CHAPTER 1: Generalities about Microstrip antennas and MIMO – Ultra Wide Band antennas

1.1 Introduction

The antenna is an essential part of any wireless system. According to the IEEE Standard Definition of terms for Antennas, an antenna is defined as "a means for radiating and receiving radio waves" [3]. In an advanced wireless system, an antenna is usually required to optimize the radiation energy in some directions and suppress it in others at certain frequencies. A good design of the antenna can relax system requirements and improve overall system performance. To describe the performance of an antenna, there are several commonly used antenna parameters, including impedance bandwidth, radiation pattern, directivity, gain, efficiency, and polarization [4]. In the present work we will deal with monopole MIMO-UWB antenna.

1.2 Microstrip patch antenna

Microstrip patch antennas are a class of planar antennas which have been researched and developed extensively in the last four decades. They have become favorites among antenna designers and have been used in many applications in wireless communication systems, both in the military sector and in the commercial sector.

1.2.1 Basic structure

The basic structure of the microstrip patch antenna is shown in Figure 1.1. It consists of area of metallization supported above a ground plane by a thin dielectric substrate and fed against the ground at an appropriate location. The patch shape can in principle be arbitrary in practice, but the rectangle, the circle; the equitriangle and the annular-ring are common shapes.

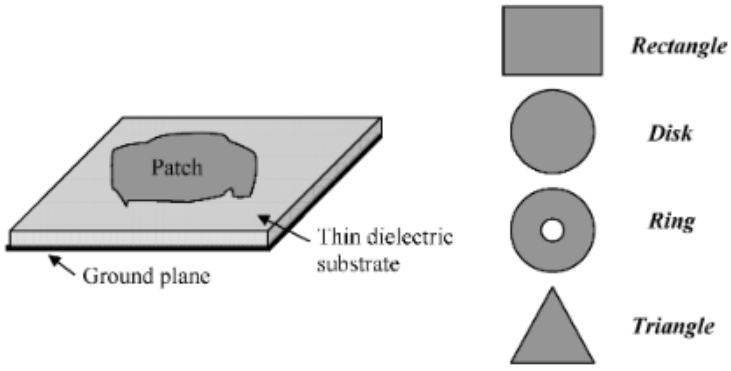

Figure 1.1: the structure of microstrip antenna [28]

1.2.2 Feeding techniques

A variety of methods can feed microstrip Patch Antenna. These methods can be classified into two categories: contacting and non-contacting. In the contacting methods, the RF power is fed directly to the radiating patch using connecting elements such as a microstrip line[5]. In a non-contacting scheme, the patch is not directly fed with the RF power, but instead power is transferred to the path from the feed line through electromagnetic coupling. The most commonly used non-contacting feed methods are aperture and proximity coupled feed.

1.2.2.1 Microstrip feed line

In this type of feed technique, a conducting strip is connected directly to the microstrip patch's edge, as shown in figure below. The conducting strip is smaller in width than the patch, and this kind of feed arrangement has the advantage that the feed can be etched on the same substrate to provide a planar structure.

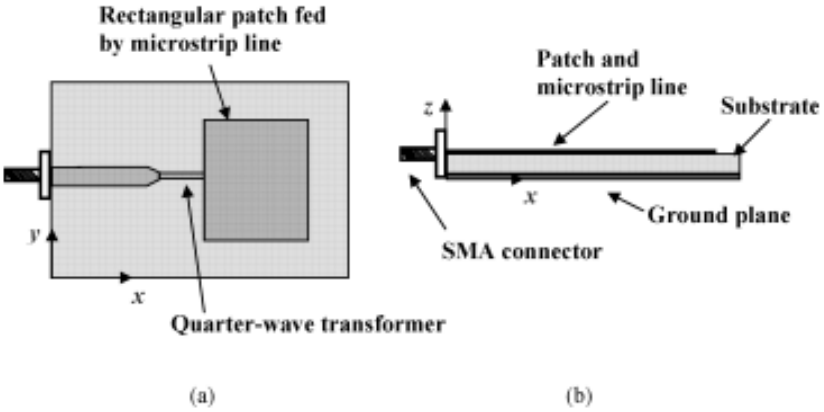

Figure 1.2 The geometry of a direct microstrip feed microstrip patch antenna (a) top view and (b) side view [28]

The purpose of the inset cut in the patch is to match the feed line's impedance to the patch without the need for any additional matching element, as in figure below.

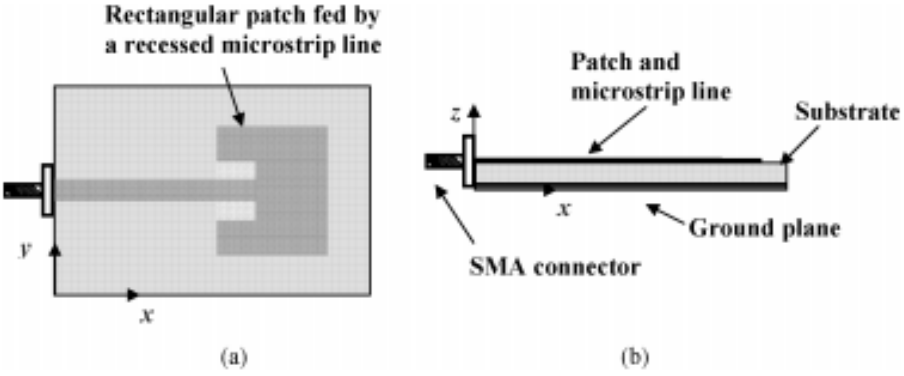

Figure 1.3 The inset in microstrip feed (a) top view and (b) side view [28]

1.2.2.2 Co-axial feed

The co-axial feed is a non-planar feeding technique in which co-axial cable is used to feed the patch. The inner conductor of the co-axial connector extends through the dielectric, making a metal contact with the patch, and the outer conductor of the cable is connected to the ground plane, as shown in figure below .The probe is in direct contact with the antenna, and it is located at the point where the antenna input is 50 ohms.

This feed method is easy to fabricate and has low spurious radiation. However, its major disadvantage is that it connected to Ground Plane Connector.

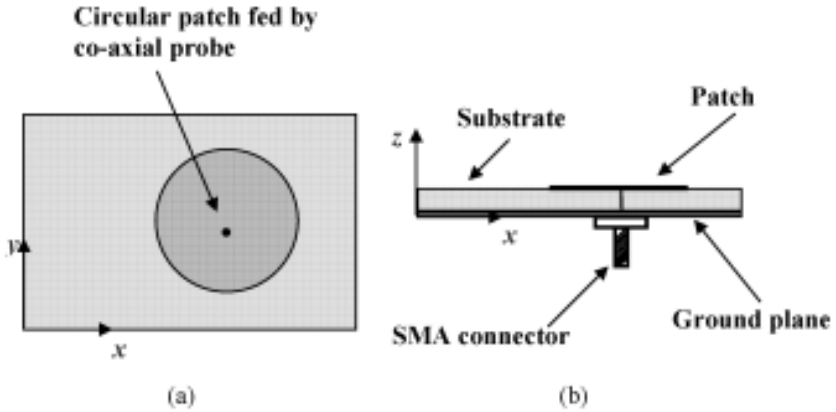

Figure 1.4 The geometry of coaxial probe feed microstrip patch antenna (a) top view and (b) side view [28].

1.2.2.3 Aperture coupled feed

The aperture feed technique consists of two dielectric substrates, namely antenna dielectric substrate, and feed dielectric substrate. These dielectric substrates are separated by a ground plane, which has a slot at its center. The metal patch is placed on top of the antenna substrate is shown in figure below. The ground plane is placed on the other side of the antenna dielectric. The feed dielectric and feed line are placed on the other side of the ground plane to provide isolation. Aperture feed provides excellent polarization purity, which is something unattainable with other feed techniques. Aperture fed antenna offers higher bandwidth. It is very useful in applications in which we do not want to use wires from one layer to another. The disadvantage with this feed is that it requires multilayer fabrication.

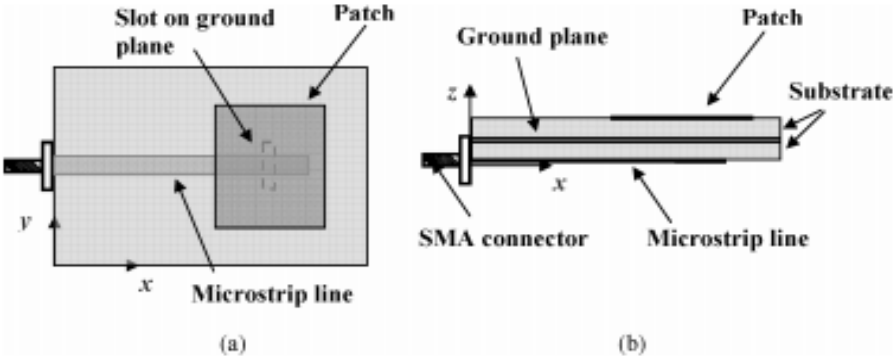

Figure 1.5 Geometry of aperture coupled feed microstrip patch antenna (a) top view and (b) side view [28].

1.2.2.4 Proximity coupled feed

In proximity feed, the feed line is placed between two dielectric substrates. In the edge fed technique, it is impossible to choose a 50 ohms feed point since the impedance at the edges will be very high. To overcome this, the feed line is moved to a lower level below the patch. The edge of the feed line is located at a point where the antenna input impedance is 50 ohms. Here the power transfer from the feed to the patch takes place through electromagnetic field coupling. Since the feed line has been moved to a lower level, feed line radiation has been reduced to a great extent, and also, this technique allows planar feeding. Also, it has an improved bandwidth efficiency compared to the other techniques. The disadvantage with this method is that multilayer fabrication has to be done, and it offers poor polarization purity.

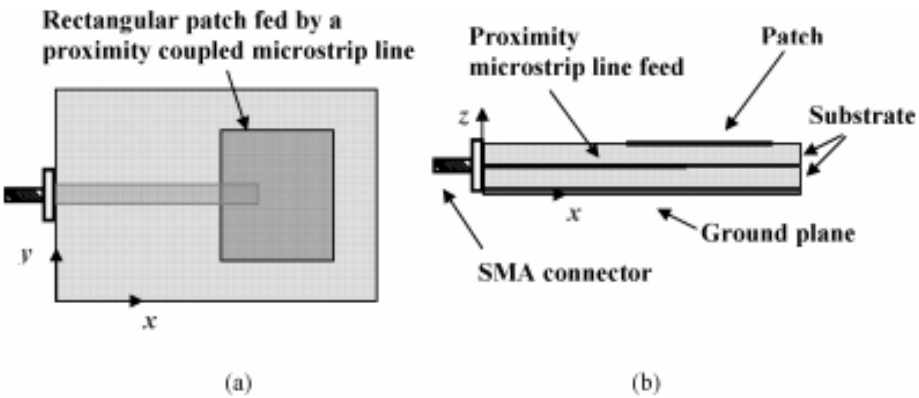

Figure 1.6 Geometry of coaxial coupled feed microstrip patch antenna (a) top view and (b) side view [28].

1.2.3 Radiation mechanism

The radiation mechanism can be simply explained using the cavity model. When the microstrip is provided with power, a charge distribution is set up on the upper and lower surface of the patch and the bottom of the ground plane, as shown in the figure below. This charge distribution is controlled by two mechanisms: an attractive mechanism and a repulsive

mechanism. The attractive mechanism is between the opposite charge on the bottom side of the patch and the ground plane, which keeps the charge concentration intact at the bottom of the patch. On the other hand, the repulsive mechanism between the like charge on the bottom of the patch causes pushing some charges from the bottom to the top of the patch. The charge movements create currents flowing at the top and bottom surface of the patch.

The cavity model assumes that the substrate height to patch width ratio is very small allowing the attractive mechanism to dominate leading to most of the charge concentration and the current to be below the patch surface.

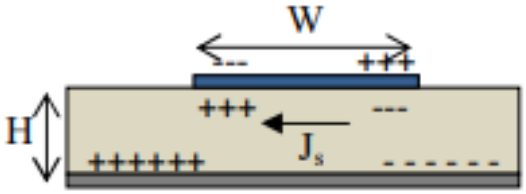

Figure 1.7 Charge distributions on a microstrip antenna

1.2.4 Antenna parameters

Antenna parameters are essential for selecting and using antennas in virtually all applications. These applications include antenna testing, electromagnetic compatibility (EMC), telecommunication and more. There are a variety of standardized methods for describing antenna parameters.

1.2.4.1 Return loss (S_{11})

Return loss is an important parameter for antennas and it was first used in the telephone industry to measure the "echo" on the various bidirectional circuits and lines. It is simply the logarithmic ratio of relative magnitudes of input power and reflected power [6]:

$$RL\ (dB) = 20\log(\Gamma) \tag{1.1}$$

1.2.4.2 Input impedance

The input impedance is defined as "the impedance presented by an antenna at its terminals or the ratio of the voltage to current at a pair of terminals or the ratio of the appropriate components of the electric to magnetic fields at a point. The ratio of the voltage to current at these terminals, with no load attached, defines the impedance of the antenna as[7]:

$$Z_A = R_A + jX_A \tag{1.2}$$

R_A: The real part of Z_A

X_A: The imaginary part of Z_A

1.2.4.3 voltage standing wave ratio (VSWR)

The VSWR is basically a measure of the impedance mismatch between the feeding system and the antenna. The higher the VSWR the greater is the mismatch. The minimum possible value of VSWR is unity and this corresponds to a perfect match. It is shown as[8]:

$$\boldsymbol{VSWR} = \frac{\boldsymbol{V_{max}}}{\boldsymbol{V_{min}}} = \frac{\mathbf{1}+|\boldsymbol{\Gamma}|}{\mathbf{1}-|\boldsymbol{\Gamma}|} \quad (1.3)$$

Where the reflection coefficient is:

$$\boldsymbol{\Gamma} = \frac{\boldsymbol{Z_{in}}-\boldsymbol{Z_0}}{\boldsymbol{Z_{in}}+\boldsymbol{Z_0}} \quad (1.4)$$

Where **Zin** is the input impedance of the antenna and **Zo** denotes the characteristic impedance of the feed line, **Zo** of the assumed feed line is equal to 50 Ohms.

1.2.4.4 Resonance Frequency

The resonance frequency is the frequency where the capacitive and inductive reactances cancel each other out. At this point the antenna appears purely resistive, the resistance being a combination of the los

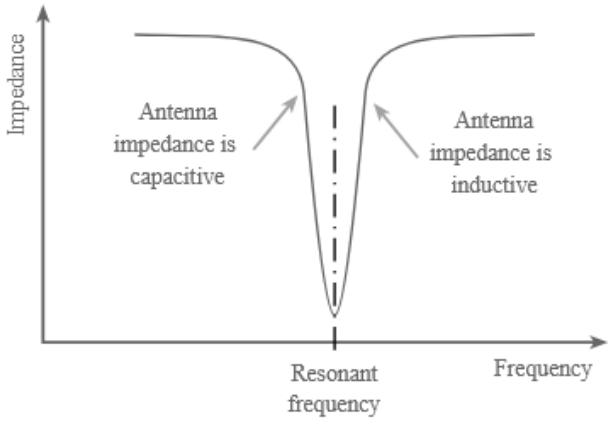

Figure 1.8 The resonance frequency

1.2.4.5 Bandwidth

In antenna terminology, the frequency bandwidth of a narrow band antenna is generally characterized with either the lower and upper limits of frequency band (f_l and f_u) or the percentage (%) bandwidth for a center frequency, which is given as [9]:

$$\boldsymbol{Bandwidth}(\%) = \frac{\boldsymbol{f_u}-\boldsymbol{f_l}}{\boldsymbol{f_r}} \times \mathbf{100} \quad (1.5)$$

Where, f_r is the resonance frequency.

1.2.4.6 Directivity

The directivity of an antenna is the measurement of the highest amount of radiated power in a direction divided by the average power of an antenna radiated in all directions. Hence, a high directivity antenna will have a beam pattern that is very strong in a single direction, where an antenna with lower directivity will have greater amounts of beam energy outside of the main lobe. The envelope of an antenna may also be described in terms of the half power beamwidth, otherwise known as the 3 dB beamwidth. The 3 dB beamwidth is the angular width of the radiation pattern between the two points 3 dB below the peak beam.
Where the mathematical form is[9]:

$$\boldsymbol{D = \frac{U}{U_0} = 4\pi \frac{U}{P_{rad}}} \tag{1.6}$$

1.2.4.7 Gain and Efficiency

Antenna gain is a relative parameter that describes the amount of power transmitted in the main direction of the antenna in respect to an isotropically radiating source. For instance, an antenna with a 6 dB antenna gain would receive 6 dB greater powers than an isotropic antenna in the same position. Antenna gain may also be given in terms of dBi, which is dB relative to an isotropic antenna, but may also be given as dBd, which is dB relative to a dipole antenna (2.15 dBi).

This is not to be confused with antenna efficiency, which is a ratio of the power input to an antenna compared to the amount of power radiated from an antenna. Efficiency is often given as a percentage, a decimal or in dB, but is just a ratio with a value between zero and one. Antenna efficiency should also not be confused with antenna voltage standing wave ratio (VSWR) or reflection coefficient, which is related to the impedance match of the antenna ports to the interconnect and/or source. An antenna may be measured in terms of total efficiency, which is merely a multiplication of antenna radiation efficiency and loss from impedance mismatch[9].

1.2.4.8 Radiation pattern

Another feature of an antenna that changes with frequency is its radiation pattern. In the case of a beam it is particularly noticeable. In particular the front to back ratio will fall off rapidly outside a given bandwidth, and so will the gain. In an antenna such as a Yagi this is caused by a reduction in the currents in the parasitic elements as the frequency of operation is moved away from resonance. For beam antennas such as the Yagi the radiation pattern bandwidth is

defined as the frequency range over which the gain of the main lobe is within 1 dB of its maximum[9].

For many beam antennas, especially high gain ones it will be found that the impedance bandwidth is wider than the radiation pattern bandwidth, although the two parameters are inter-related in many respects.

1.2.4.9 The polarization

Antenna polarization is a description of the way the electric field (E-field) or magnetic field (H-field) of a wave front oscillates. If the field lines oscillate within a single axis, they are known as linearly polarized. A linear polarized antenna may be horizontal (0°), vertical (90°) or cross polarized if at an angle other than 0° or 90°. An elliptical polarization is obtained when the field oscillations of the wave front orbit around the origin and are either travelling clockwise (right hand elliptically polarized) or counter clockwise (left hand elliptically polarized). As a special case of elliptical polarization, the E-field lines may perfectly rotate around the origin and form a circle, which is known as circular polarization[10].

It is important to have receiving and transmitting antennas with matched polarization, or some of the power of the signal will be lost due to the polarization mismatch. This is known as the polarization loss factor (PLF), which can be described with the equation[10]:

$$PLF = \cos^2 \varphi \tag{1.7}$$

$\boldsymbol{\varphi}$ is the angle offset of the polarization of the antenna compared to the polarization of the wave fro

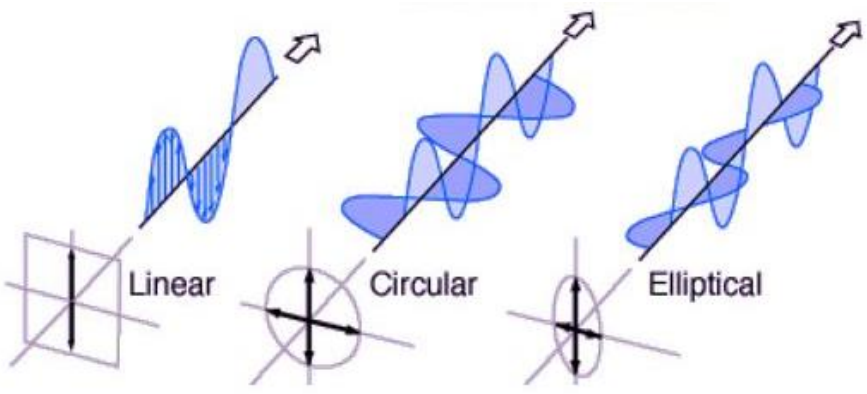

Figure1.9 polarization of the antenna [10]

❖ **Parasitic components of polarization**

An antenna is said to have good polarization purity if the level of the cross-polarization component, noted E_{cross}, is at least –20 dB lower than the co-polar component. The Ludwing definition of the two components of an antenna polarized along the Oy axis give [11]:

$$\begin{bmatrix} E_{co} \\ E_{cross} \end{bmatrix} = \begin{bmatrix} +\sin\varphi & +\cos\varphi \\ +\cos\varphi & -\sin\varphi \end{bmatrix} \begin{bmatrix} E_{\theta} \\ E_{\varphi} \end{bmatrix} \quad (1.8)$$

If the antenna is polarized along the Ox axis, the Eco and E_{cross} are expressed as:

$$\begin{bmatrix} E_{co} \\ E_{cross} \end{bmatrix} = \begin{bmatrix} +\cos\varphi & -\sin\varphi \\ +\sin\varphi & +\cos\varphi \end{bmatrix} \begin{bmatrix} E_{\theta} \\ E_{\varphi} \end{bmatrix} \quad (1.9)$$

1.3 MIMO- Ultra Wide Band antenna:

With the development of wireless communication systems, high data rates and large channel capacity have been extensively studied by researchers in the past years. Ultra Wide Band (UWB) technology has drawn considerable attention for its high data rate, wide bandwidth, and low cost. Due to the low transmission power, UWB technology is widely used in the field of short-range communications, radar, positioning, and tracking. Diversity technology is utilized in the multiple-input multiple-output (MIMO) system to enable data transmission, thus effectively suppressing multipath fading and improving channel capacity[12]. In recent years, scholars have combined UWB technology with MIMO technology to develop UWB-MIMO technology. UWB-MIMO technology makes full use of UWB and MIMO's advantages, effectively improving channel capacity and data rates and suppressing multipath fading. As an essential part of wireless communication systems, antennas are particularly important for UWB-MIMO communication systems. Therefore, UWB-MIMO antennas have attracted extensive attention and researches from scholars.

1.3.1 Specific parameters for UWB antennas:

In UWB systems, the previous fundamental and classical parameters must be considered in designing antennas but there are more challenges to monitor them and some additional parameters.

1.3.1.1 Bandwidth:

First of all, what distinguishes a UWB antenna from other antennas is its ultra-wide frequency range. According to the FCC's definition, a suitable UWB antenna should be able to yield an absolute bandwidth of not less than 500 MHz or a fractional bandwidth of at least 0.2[13].

$$\boldsymbol{Bandwidth}(\%) = \frac{f_u - f_l}{fc} \times \mathbf{100} \quad (1.9)$$

1.3.1.2 Radiation Pattern

Directional or omnidirectional radiation properties are needed depending on the practical application. Omni-directional patterns are normally desirable in mobile and hand-held systems. For radar systems and other directional systems where high gain is desired, directional radiation characteristics are preferred. High radiation efficiency is usually required for antennas but it is imperative and essential for an ultra wide band antenna because the transmit power spectral density is excessively low. Therefore, any excessive losses incurred by the antenna could potentially compromise the functionality of the system [14].

1.3.1.3 Impulse Response

As the origin of UWB technology stems from time-domain electromagnetic, therefore UWB antenna is required to achieve good time domain characteristics (i.e., good impulse response). The idea is simply to characterize the LTI(Linear Time Invariant) system by its response to an impulsive excitation instead of amplitude and phase and measurements versus frequency (i.e., swept frequency response).UWB systems often employ extremely short pulses for data transmission[15].

1.3.1.4 Group Delay

It is an important parameter that represents the degree of distortion of UWB signal. Group delay is a measure of the slope of the transmission phase response. The linear portion of the phase response is converted to a constant value and deviation from linear phase is transformed into deviations from constant group delay. The variations in group delay cause signal distortion, just as deviations from linear phase cause distortion. It can be given as:

$$groupe\ delay = -\frac{\Delta\emptyset}{\Delta\omega} \tag{1.11}$$

Where φ is the total phase shift in radians, andω is the angular frequency in radians per unit time, equal to $2\pi f$, where $f$is the frequency. The group delay variations induced by the radiation pattern of the antenna will affect the overall receiver system performance, since it can bring relatively large timing errors. An antenna gain versus frequency without nulls, means a linear phase response, hence a constant group delay [14].

1.3.1.5 Compliance with Spectral Masks

A good design of UWB antenna should be optimal for the performance of overall system. To avoid the possible in band/out band interference between the UWB systems and existing

electronic systems, the antenna should be designed such that the overall device (antenna and RF front end) complies with the mandatory power emission mask given by the FCC or other regulatory bodies [14].

1.3.1.6 Size and Cost

A suitable antenna needs to be small and of light weight enough to be compatible to the application [14].

1.3.2 Specific parameters for MIMO antennas

Like the case of UWB, there are also some additional parameters other than the fundamental parameters to be taken into account while designing MIMO antennas.

1.3.2.1 Mutual Coupling and Isolation

In MIMO applications, the signals transmitted by multiple antenna elements are generally supposed to be independent or uncorrelated. But in reality, the current induced on one antenna produces a voltage at the terminals of nearby elements, termed as mutual coupling [16]. It means there is always mutual coupling present between nearby antenna elements. However, for MIMO applications, the mutual coupling should be minimized to as low value as possible. The port-to-port isolation is defined as the transmission of power between two of the input ports of the multiport antenna under test [16]. It is characterized by $|S_{21}|$ parameter. It must be noted that isolation is a positive quantity and is given as:

$$Isolation = -10\log_{10}|S_{21}|^2 \tag{1.12}$$

In MIMO systems, to maximize the energy radiated by an antenna, it should be ensured that negligible amount of transmitted energy is lost into the ports of other antennas terminated by the matched impedances. In other words, MIMO systems require the $|S_{21}|$ to be minimized to as low value as possible as isolation is directly related to the antenna efficiency[14].

1.3.2.2 Mean Effective Gain

The performance of MIMO systems is also characterized by the mean effective gain (MEG) of the antennas. The MEG is a statistical measure of the antenna gain that can be defined as the ratio of the mean received power of the antenna and the total mean incident power. It can be expressed by the following equation[17]:

$$MEG = \int_0^{2\pi}\int_0^{\pi}\left(\frac{XPR}{1+XPR}G_\theta(\theta,\varphi)P_\theta(\theta,\varphi) + \frac{1}{1+XPR}G_\varphi(\theta,\varphi)P_\varphi(\theta,\varphi)\right)\sin\theta d\theta d\varphi \tag{1.13}$$

Where P_θ and P_φ are the angular diversity functions of the incident power with respect to θ and φ directions respectively, G_θ and G_φ are the gains with respect to θ and φ directions respectively, and XPR represents the cross-polarization power gain which is defined as:

$$XPR = \frac{\int_0^{2\pi}\int_0^{\pi} P_\theta(\theta,\varphi)\sin\theta d\theta d\varphi}{\int_0^{2\pi}\int_0^{\pi} P_\varphi(\theta,\varphi)\sin\theta d\theta d\varphi} \quad (1.14)$$

The MEG is a normalized measure of the received power, where the powers (either P_θ or P_φ) are normalized as[18]:

$$\int_0^{2\pi}\int_0^{\pi} P_\theta(\theta,\varphi)\sin\theta d\theta d\varphi = 1 \quad (1.15)$$

and the gains are normalized in such a way that

$$\int_0^{2\pi}\int_0^{\pi} (G_\theta(\theta,\varphi) + G_\varphi(\theta,\varphi))\sin\theta d\theta d\varphi = 4\pi \quad (1.16)$$

In the case where the antenna is located in a totally random channel environment, the value of XPR is 1 and $P_\theta = P_\varphi = \frac{1}{4\pi}$. Then, MEG can be calculated using (1.12) as follows:

$$MEG = \int_0^{2\pi}\int_0^{\pi} \left(\frac{1}{1+1}\frac{1}{4\pi} G_\theta(\theta,\varphi) + \frac{1}{1+1}\frac{1}{4\pi} G_\varphi(\theta,\varphi)\right)\sin\theta d\theta d\varphi = \frac{1}{2} \quad (1.17)$$

The MEG is then equal to the total antenna efficiency divided by two or -3 dB[19] and it is independent of the radiation patterns. In order to achieve good diversity gain, the ratio of the MEG between the two antennas should close to unity in order to ensure that average received power by each antenna is nearly equal [20].

1.3.2.3 Correlation Coefficient

The correlation coefficient is a parameter of great importance for the systems providing diversity. The signals received in the diversity systems can be correlated to some extent. The correlation coefficient is a mathematical and statistical tool that measures the degree of similarity among the received signals. Its modulus varies from 0to 1. Ideally, diversity systems require a correlation coefficient of zero or low by default. This parameter can be viewed by three ways: complex, envelope and power correlation coefficients. Complex correlation coefficient gives the complex measure of correlation between received signals at the antennas. It can be given as[18]:

$$\rho_c = \frac{\int_0^{2\pi}\int_0^{\pi}\left(XPRE_{\theta k}(\theta,\varphi)E^*_{\theta l}(\theta,\varphi)P_\theta(\theta,\varphi)+E_{\varphi k}(\theta,\varphi)E^*_{\varphi l}(\theta,\varphi)P_\varphi(\theta,\varphi)\right)\sin\theta d\theta d\varphi}{\sqrt{\sigma_k^2\sigma_l^2}} \quad (1.18)$$

Where σ_k^2 and σ_l^2 represent the variances of k^{th} and l^{th} branches and can be written mathematically as:

$$\rho_c = \int_0^{2\pi}\int_0^{\pi}\left(XPRG_{\theta k}(\theta,\varphi)P_\theta(\theta,\varphi) + G_{\varphi k}(\theta,\varphi)P_\varphi(\theta,\varphi)\right) \quad (1.19)$$

Also

$$G_{\theta k}(\theta,\varphi) = E_{\theta k}(\theta,\varphi)E^{*}_{\theta l}(\theta,\varphi) \quad (1.20)$$

$$G_{\varphi k}(\theta,\varphi) = E_{\varphi k}(\theta,\varphi)E^{*}_{\varphi l}(\theta,\varphi) \quad (1.21)$$

Where $E_{\theta k}$ and $E_{\varphi k}$ are complex electric fields in the directions θ and φ respectively for thek^{th}antenna. Similar expressions are valid for l^{th}antenna. Usually, the envelope correlation is presented to evaluate the diversity capabilities of MIMO systems[21]. This parameter is always real and by definition gives the correlation among the amplitudes of the signals at antennas. For Rayleigh fading channel, the envelope correlation can be given as follows:

$$\rho_e = |\rho_c|^2 \quad (1.22)$$

It is clear that correlation should be preferably computed from 3D radiation patterns but it becomes tedious. However, assuming that the diversity system will operate in a uniform multipath environment, the correlation coefficient can be calculated from S-parameters using the following equation [22]:

$$\rho_e = \left|\frac{S^{*}_{11}S_{12}+S^{*}_{21}S_{22}}{\sqrt{1-|S_{11}|^2-|S_{21}|^2}.\sqrt{1-|S_{22}|^2-|S_{12}|^2}}\right| \quad (1.23)$$

It offers a simple procedure compared to the radiation pattern approach, but it should be emphasized that this equation is strictly valid when the following assumptions are fulfilled[14]:

- Antennas should have high efficiency and no mutual losses.
- Antenna system is positioned in a uniform multipath environment which is not strictly the case in real environments; however, the evaluation of some prototypes in different real environments has already shown that there are no major differences in these cases.
- Load termination of the non-measured antenna is 50Ω. In reality, the radio front-end module does not always achieve this situation, but the 50 Ω evaluation procedure is commonly accepted.

All these limitations are clearly showing that in real systems the envelope correlation calculated based on of the help of theS_{ij}parameters is not the exact value, but neverthelessis a good approximation. In addition, it should be noted that antennas with an envelope correlation coefficient less than 0.5 are recognized to provide significant diversity performance.

1.3.2.4 Diversity Gain

The diversity gain (DG) is a figure of merit used to quantify the performance level of diversity techniques. The DG is the slope of the error probability curve in terms of the received SNR in a log-log scale. However, the DG can also be defined as the increment of the

SNR at a given probability, normally 1% or 10%. Such DG can easily be calculated by looking at the cumulative distribution function (CDF) curves of the SNR, and comparing the combined SNR using some specific diversity technique with the SNR of an un-coded SISO communication system. Mathematically, it can be expressed as:

$$DG = \frac{(SNR)_c}{(SNR)_r} \tag{1.24}$$

where indices "c" and "r" are used for the combined and the reference[23]. Depending on the reference CDF, it is possible to write three definitions for the diversity gain: (23)

- Apparent diversity gain: difference between power levels in dB (at certain CDF level),between CDF of combined signal, and CDF of signal at the port with the strongest average signal levels.
- Effective diversity gain: difference between power levels in dB (at certain CDF level), between CDF of combined signal, and CDF of signal at the port of an ideal single antenna (corresponding to radiation efficiency of 100%), measured in the same environment.
- Actual diversity gain: difference between power levels in dB (at certain CDF level), between CDF combined signal, and CDF of signal at the port of an existing practical single antenna that is to be replaced by the diversity antenna under test, measured at the same location (for example, relative to a head phantom).

The DG is also related to the correlation coefficient. The relation between DG and correlation coefficient can be given approximately by:

$$DG = 10\sqrt{1 - |\rho|^2} \tag{1.25}$$

This relationship clearly shows that the lower the correlation coefficient the higher will be the diversity gain. Therefore, high isolation is required between the antennas otherwise the DG will be low. Further, whatever the combining method is being used, the maximum diversity gain is obtained when the correlation coefficient is zero [24].

1.3.2.5 Total Active Reflection Coefficient

The reflection coefficient does not accurately characterize the radiation efficiency and bandwidth of a MIMO antenna. Instead of simple reflection coefficient, the array's total active reflection coefficient (TARC) can be used so that it accounts for both coupling and random signal combination. Thus, TARC provides a more meaningful measure of MIMO efficiency. For a desired port excitation, summation of the available power at all excitation ports is assumed as incident power, radiated power as transferred power, and the difference between

these two as reflected power. The square root of the ratio of reflected power and incident power is defined as the TARC[25], mathematically given by:

$$\Gamma_a^t = \frac{available\ power - radiated\ power}{available\ power} \tag{1.26}$$

For instance, TARC for a lossless N-port antenna can be described as:

$$\Gamma_a^t = \sqrt{\sum_{i=1}^{N} |b_i|^2} \Big/ \sqrt{\sum_{i=1}^{N} |a_i|^2} \tag{1.27}$$

Where $[b] = [S] \cdot [a]$, a_i is the incident signal vector with randomly phased elements and b_i is the reflected signal vector.

Furthermore, for 2×2 network, the scattering matrix can be written as:

$$\begin{pmatrix} b_1 \\ b_2 \end{pmatrix} = \begin{pmatrix} S_{11} S_{12} \\ S_{21} S_{22} \end{pmatrix} \begin{pmatrix} a_1 \\ a_2 \end{pmatrix} \tag{1.28}$$

It can be assumed that the reflected signal will be randomly phased with independent and identical distributed Gaussian random variables because MIMO channels are assumed as Gaussian and multipath spread in the propagation channel. Since sum or difference of independent Gaussian random variables is Gaussian, reflected signals are characterized as:

$$b_1 = S_{11} a_1 + S_{12} a_2 = S_{11} a_0 e^{j\theta_1} + S_{12} a_0 e^{j\theta_2} = a_1 (S_{11} + S_{12} e^{j\theta}) \tag{1.29}$$

$$b_2 = S_{21} a_1 + S_{22} a_2 = S_{21} a_0 e^{j\theta_1} + S_{22} a_0 e^{j\theta_2} = a_1 (S_{21} + S_{22} e^{j\theta}) \tag{1.30}$$

Therefore, TARC for two-port antenna can be described as follows[26]:

$$\Gamma_a^t = \sqrt{\frac{|S_{11} + S_{12} e^{j\theta}|^2 + |S_{21} + S_{22} e^{j\theta}|^2}{2}} \tag{1.31}$$

The TARC of MIMO antenna is calculated by applying different combinations of excitation signals to each port. There is no need to define the TARC as a complex number since the phase reference plane does not have any physical meaning for a multiport antenna. The TARC is a real number between zero and one. When the value of the TARC is equal to zero, all the delivered power is radiated and when it is equal to one, all the power is either reflected back or goes to the other ports.

1.4 Conclusion

In this chapter the Microstrip antenna and the MIMO-UWB antenna have been introduced and the most important antenna parameters have been presented. In the next chapter we will see the design and the analysis of a rectangular MIMO Antenna.

CHAPTER 2

Rectangular Monopole Antenna

CHAPTER 2: Rectangular Monopole Antenna

2.1 Introduction

A rectangular shaped Monopole antenna is designed to operate in UWB applications using transmission line model, excited using a waveguide port. All designs and simulations have been completed using CST microwave studio.

2.2 Rectangular Monopole antenna

The rectangular monopole patch antenna, as shown in figure 2.1, is one of the most used configurations in the antenna design for its simplicity in analysis and fabrication.

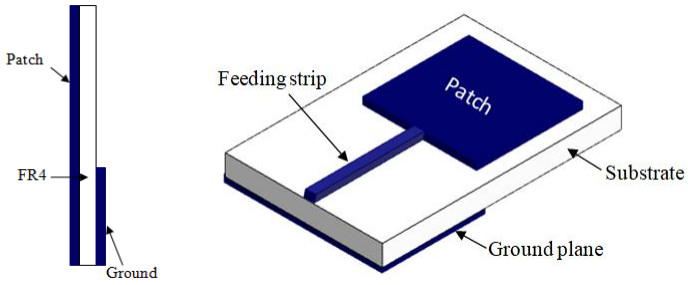

Figure 2.1 Rectangular Monopole patch antenna

2.2.1 Design procedure and Simulation results

2.2.1.1 Design specifications

A rectangular antenna with microstrip feed using the FR-4 substrate with relative dielectric permittivity $\varepsilon_r = 4.3$, loss tangent $tan\delta = 0.017$ and thickness $h = 1.6\,mm$ is designed as shown in Figure 2.2. For the ultra wideband WLAN application, and for purpose of keeping the antenna size moderately small a design frequency of $f_r = 5.8\,GHz$ is selected.

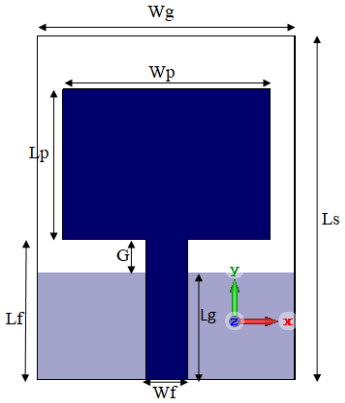

Figure2.2 Geometry of the monopole rectangular patch antenna

The basic steps for the development of rectangular patch antenna (RPA) are [1]:

Step 1: The width of the radiating RPA can be calculated with this equation:

$$W = \frac{c}{2f_r}\sqrt{\frac{2}{\varepsilon_r+1}} \tag{2.1}$$

Step 2: The effective dielectric constant of the RPA is determined as:

$$\varepsilon_{eff} = \frac{\varepsilon_r+1}{2} + \frac{\varepsilon_r-1}{2}\left(\frac{1}{\sqrt{1+\frac{2h}{w}}}\right) \tag{2.2}$$

Step 3: The effective length is specified at the resonance frequency:

$$L_{eff} = \frac{c}{2f_r\sqrt{\varepsilon_{eff}}} \tag{2.3}$$

Step 4: Extension length of the RPA compute with this equation:

$$\Delta L = h \times 0.412 \times \frac{(\varepsilon_{eff}+0.3)\left(\frac{w}{h}+0.264\right)}{(\varepsilon_{eff}-0.258)\left(\frac{w}{h}+0.8\right)} \tag{2.4}$$

The length L of the RPA is calculated as:

$$L = L_{eff} - 2\Delta L \tag{2.5}$$

Using the above formulas, the monopole dimensions are obtained as W = 15.87 mm and $L = 11.88\,mm$. The width of the feed must be chosen so that the line impedance is $50\,\Omega$ so $Wf = 3.13mm$ and the other parameters are arbitrarily chosen.

Table 2.1 displays the different dimensions of the monopole antenna

Parameters	Ws = Wg	Ls	Lg	Wp	Lp	W_f	Lf	G (gap)
Dimensions (mm)	20	27.5	11.5	15.87	11.88	3.13	12.5	1

2.2.1.2 Simulation results and discussion

2.2.1.2.1 Input reflection coefficient

Figure 2.3 depicts the simulated input reflection coefficient. It can be seen that the reflection coefficient of the considered antenna shows a good matching occurs at 3.7 GHz, the simulated −10 dB bandwidth spans a frequency range from 3.345 GHz to 4.29 GHz.

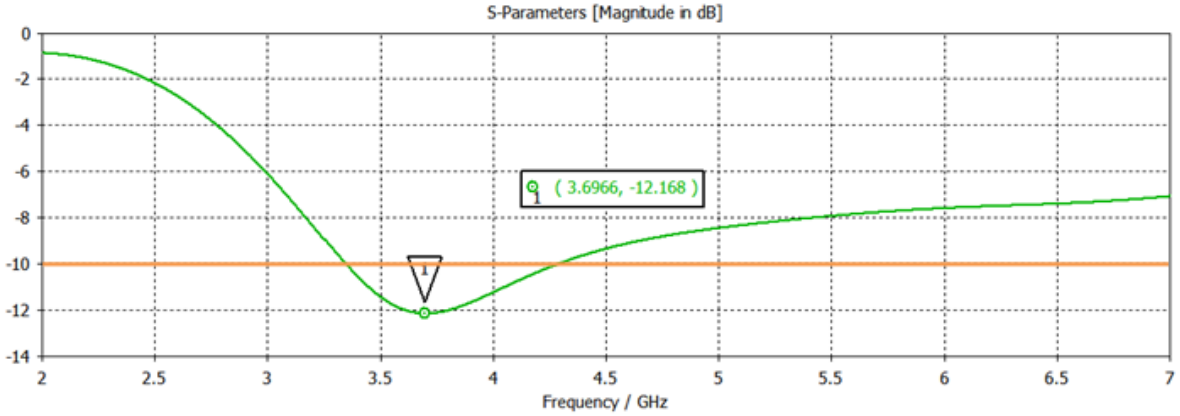

Figure 2.3 Simulated input reflection coefficient of the monopole antenna

The bandwidth (BW) of the antenna using the equation (1.11) and operating at -10 dB:

$$BW\ (\%) = \frac{4.29 - 3.345}{5.8} \times 100 = 16.29\%$$

After calculation of the bandwidth, it was found that the band is very narrow comparing to the standard bandwidth (UWB), which is insufficient for the good running of our antenna. For such raison, some adjustments are made in the antenna's width and length after performing the parametric study.

2.2.1.2.2 Parametric study

In order to understand the construction of the RPA antenna, a study was done on the effect of feed gap G and the feed line width Wf, noting that when one parameter is considered the others are kept constant.

a. Effect of the feed gap

The feed gap G is the distance between the top edge of the ground and the bottom edge of the patch, this parameter has an important effect on the bandwidth. Figure 2.4 shows the input simulated reflection coefficient curves with different values of the feed gap in order to choose the best value that achieved maximum bandwidth. From this figure it is noticed that when G becomes smaller the -10 dB bandwidth is getting narrower by losing the matching over the large bandwidth. Looking across the whole spectrum, it is clear that the value of G of 3 mm assure ultra wideband operation whereas for G of 1, 2 and 4 mm only one resonant frequency is obtained.

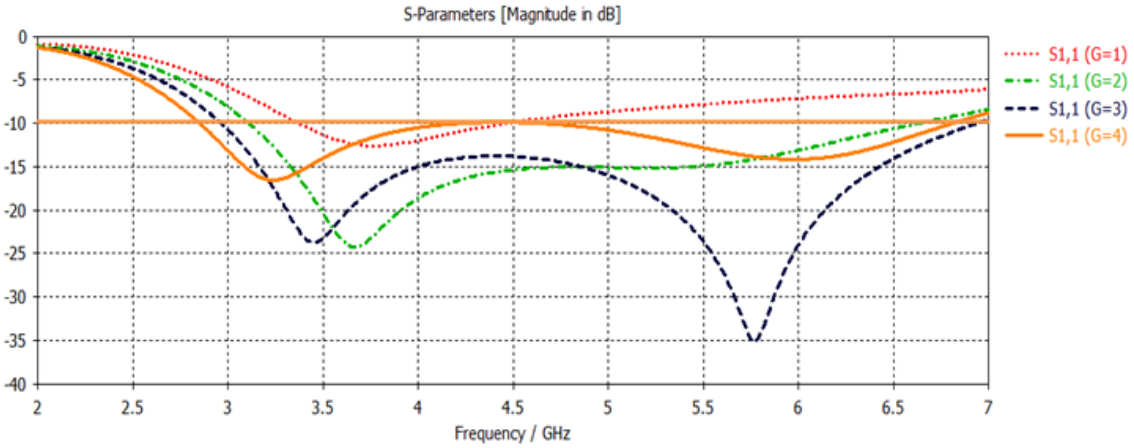

Figure 2.4 effect of the feed gap on the input reflection coefficient

b. Effect of the feed line width

The monopole rectangular antenna exhibits a broad bandwidth when the width of the feed line is at 3.08 mm. The impact of the variation of the feed line width in the better reflection coefficient of −47.12 dB and higher broadband is shown in figure below.

The parameter Wf only affects the impedance matching without the resonant frequency values.

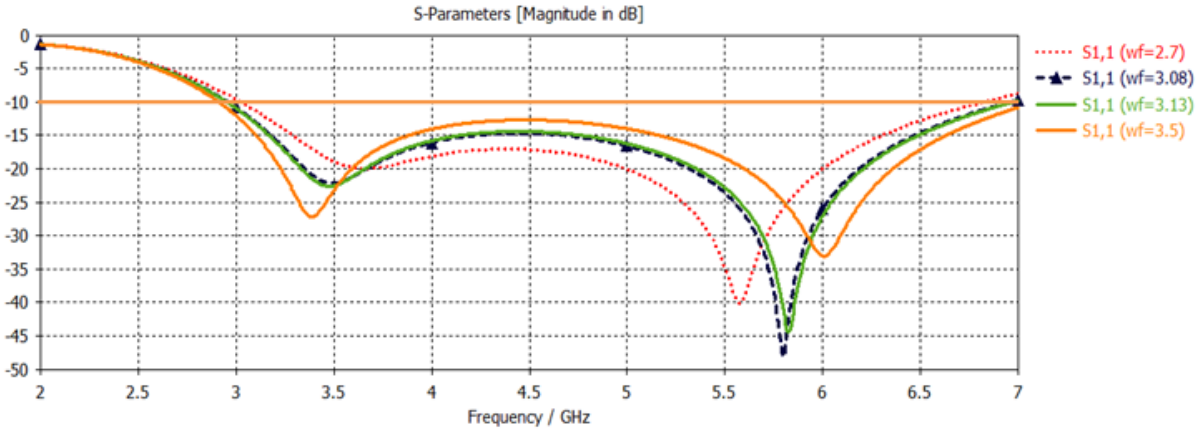

Figure 2.5 effect of the feed line width on the input reflection coefficient

Based on the above parametric study, the antenna can be adjusted to the appropriate design by proper choice of the parameter values as shown in Table 2.2.

Table 2.2 displays the different dimensions of the monopole antenna.

Parameters	Ws = Wg	Ls	Lg	Wp	Lp	W_f	Lf	G (gap)
Dimensions (mm)	20	27.5	9.5	17.72	11.45	3.08	12.5	3

2.2.1.2.3 Input reflection coefficient

As depicted in Figure 2.6, the reflection coefficient characteristic of the considered antenna shows a good matching at some frequencies, which are regarded as the resonances of the antenna. The first resonance occurs at 3.5 GHz, the second resonance at 5.8 GHz, the simulated −10 dB bandwidth spans an extremely wide frequency range from 2.965 GHz to 6.960 GHz with a percent bandwidth of : $BW\ (\%) = \frac{6.960-2.965}{6.960+2.965} \times 200\ = 80.50\%$.

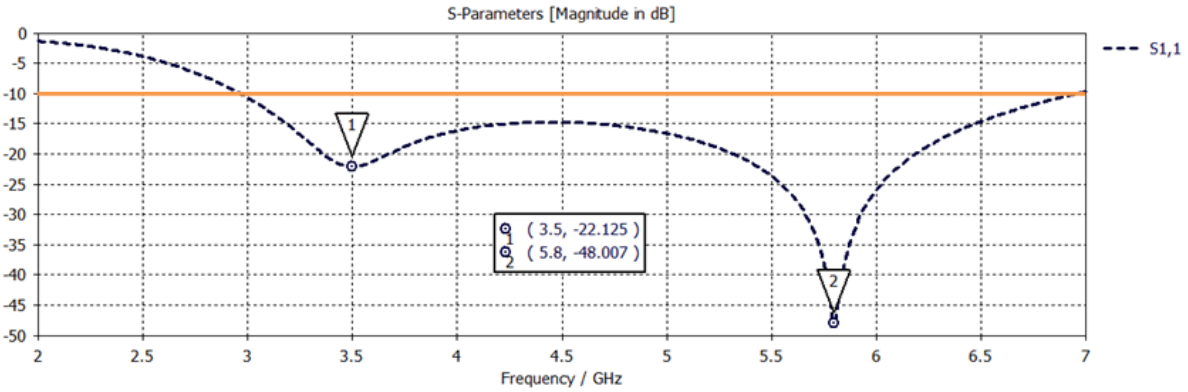

Figure2.6 Simulated input reflection coefficient of the ultra wideband monopole antenna

2.2.1.2.4 Input Impedance

The simulated input impedance of the rectangular monopole antenna is shown in Figure 2.7. The input impedance of the monopole antenna shows that the structure resonates at 3.5 GHz with a real part of 51.81 Ω and imaginary part of -7.15 Ω. The second mode is appeared at 5.8 GHz with a real part of 48.29 Ω and imaginary part of 0.30 Ω; which are very close to the line impedance (50 Ω) and this ensures a good matching with the feed line and a proper working of the antenna.

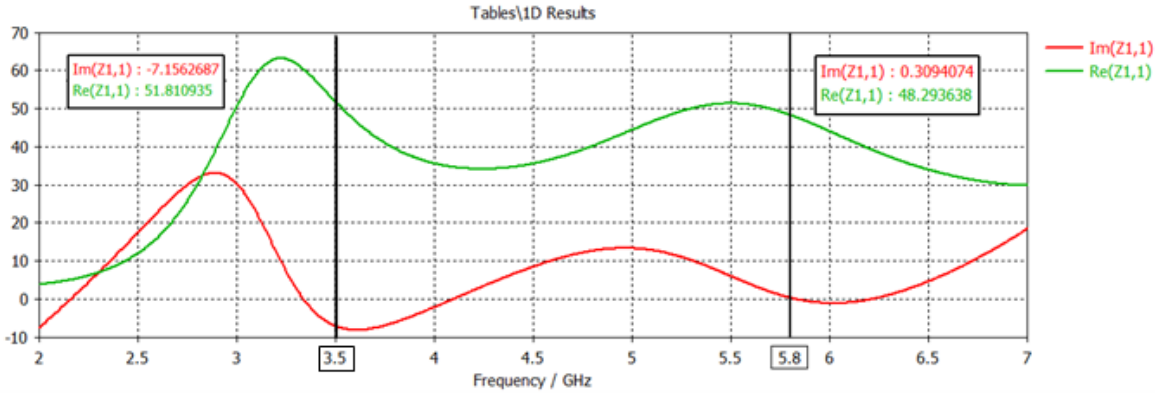

Figure 2.7 Simulated input impedance for monopole patch Antenna

2.2.1.2.5 Current distribution

The current pattern around the first resonance at 3.5 GHz is shown in Figure 2.8(a). Figure 2.8(b) shows the current pattern around the second resonance at 5.8 GHz, which indicates a second order harmonic.

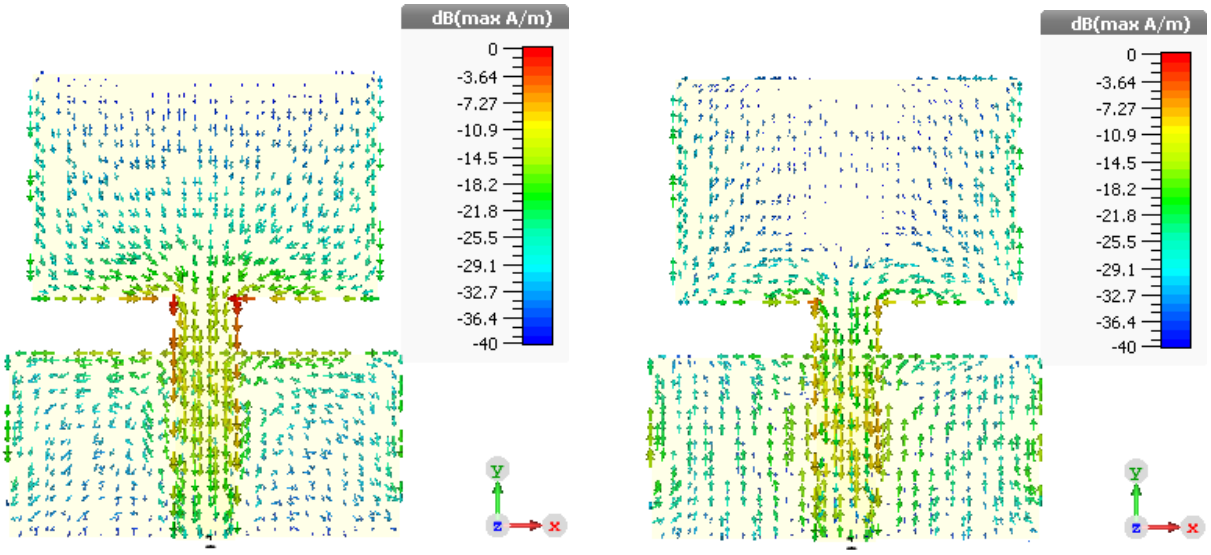

(a) **(b)**

Figure 2.8 The current distribution of the monopole antenna at (a) 3.5GHz, (b) 5.8GHz

It can be seen that many maxima appear at the higher frequency compared with the lower frequency since the antenna operates at the fundamental mode at the first frequency and higher order modes at the higher frequency with the lower wavelength.

2.2.1.2.6 Radiation Pattern

i) 2D representation of Radiation pattern

Figures 2.9, 2.10, 2.11 and 2.12 illustrate simulated 2D representations of far field radiation patterns at 3.5 GHz and 5.8 GHz respectively. Both co-polar and cross-polar components of the radiated field are drawn in the main planes, E plane and H plane, to examine polarization purity. The antenna is y-polarized since the feed line is on the y-axis. Using equation (1.8) we get:

$$E-plane: \varphi = \frac{\pi}{2} \rightarrow E_{co} = -E_{\varphi} \; and \; E_{cross} = E_{\theta}$$

$$H-plane: \varphi = 0 \rightarrow E_{co} = E_{\theta} \; and \; E_{cross} = E_{\varphi}$$

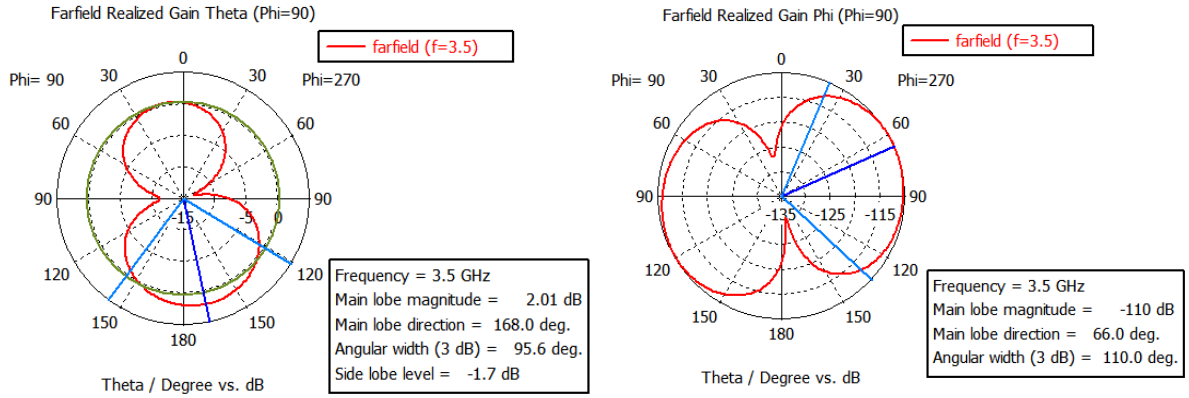

(a) (b)

Figure 2.9 E-plane radiation field pattern of the monopole antenna at 3.5 GHz
(a) co-polar , (b) cross-polar

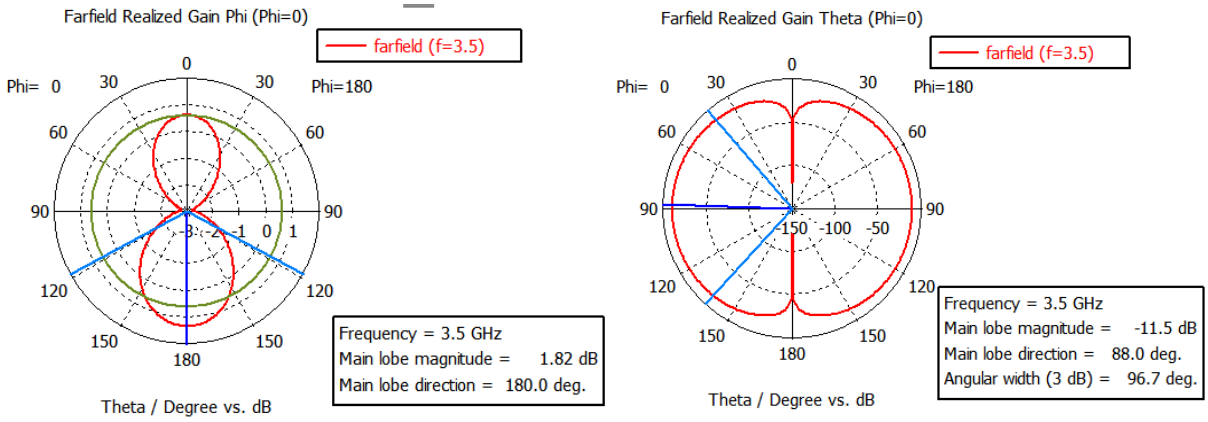

(a) (b)

Figure 2.10 H-plane radiation field pattern of the monopole antenna at 3.5 GHz
(a) co-polar , (b) cross-polar

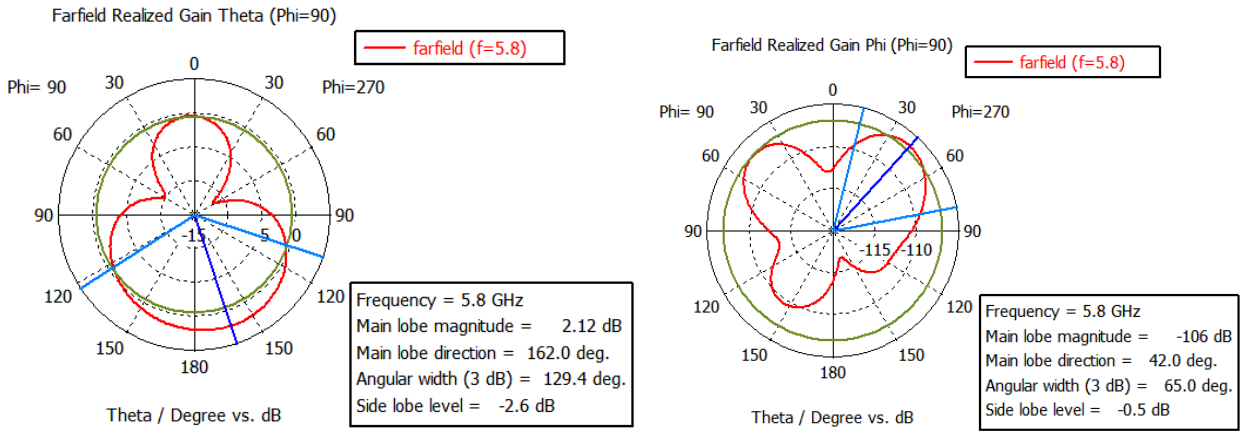

(a) (b)

Figure 2.11 E-plane radiation field pattern of the monopole antenna at 5.8 GHz
(a) co-polar , (b) cross-polar

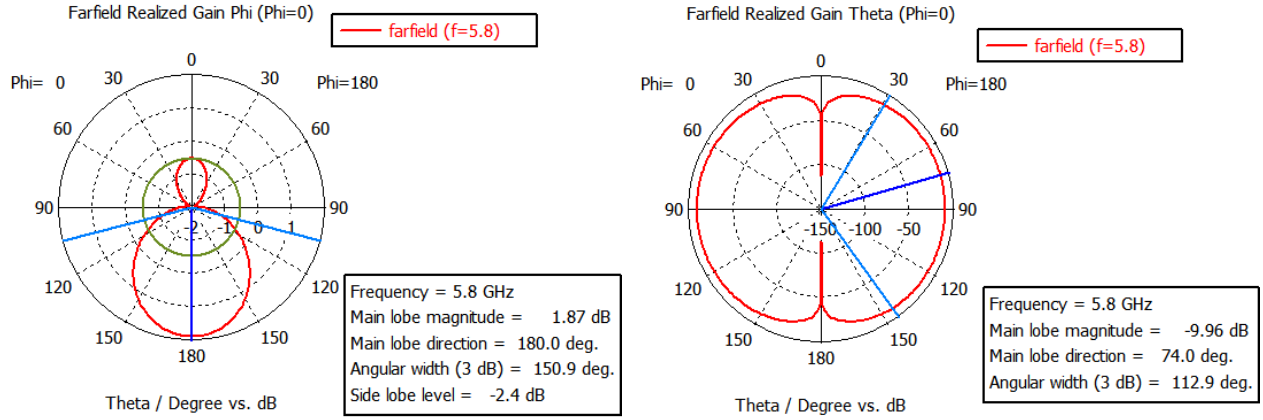

(a) (b)

Figure 2.12 H-plane radiation field pattern of the monopole antenna at 5.8 GHz
(a) co-polar, (b) cross-polar

Figure 2.9 and Figure 2.10 show that at the 3.5 GHz, the co-polar component is similar the dipole like patterns with a realized gain is 2.01 dB in the E-plane and 1.82 dB in the H-plane. The structure also shows very good polarization purity with cross-polar component level of $-112\ dB$. However, in the H-plane, the cross-polar component is only $-12.3\ dB$ lower than the co-polar.

At the 5.8 GHz, the fields are shown in Figure 2.11 and Figure 2.12; the E-plane and the H-plane respectively. In the E-plane, the co-polar component is quite pinched with realized gain is 2.12 dB and the cross-polar component with a level $-108.12\ dB$ lower than the co-polar indicates good polarization purity. For the H-plane, the co-polar component shows that the field is mainly directed toward the 180° with a gain of 1.87 dB while the cross-polar is $-11.83\ dB$ lower than the co-polar.

ii) 3D representation of Radiation pattern

Figures 2.13 and 2.14 depict the simulated 3D radiation patterns at 3.5 GHz and 5.8 GHz. At the first resonant frequency, the radiation pattern resembles a doughnut, similar to a dipole pattern, as seen in Figure 2.13. At the second harmonics, the pattern looks like a slightly pinched donut with the increasing in the gain in Figure 2.14.

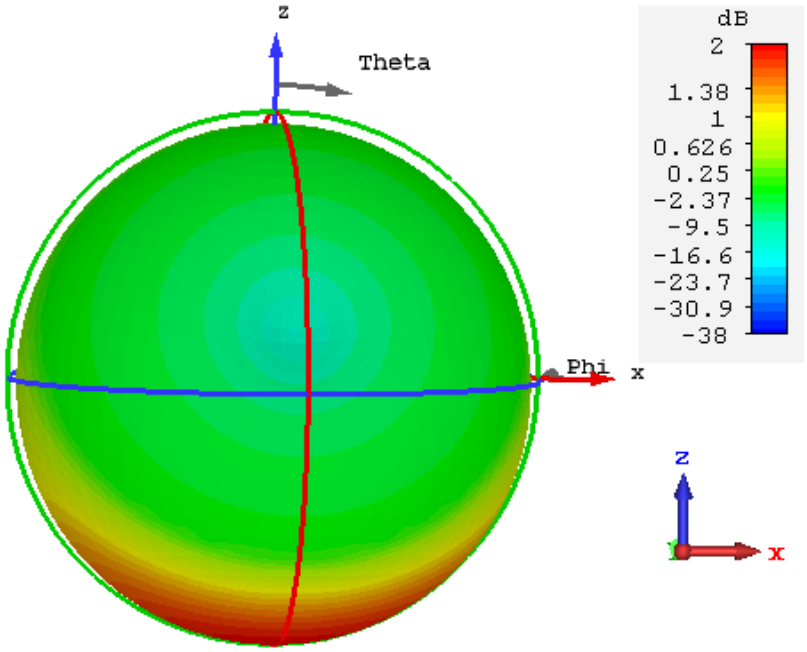

Figure 2.13 Simulated 3D radiation patterns of the proposed Antenna at 3.5 GHz

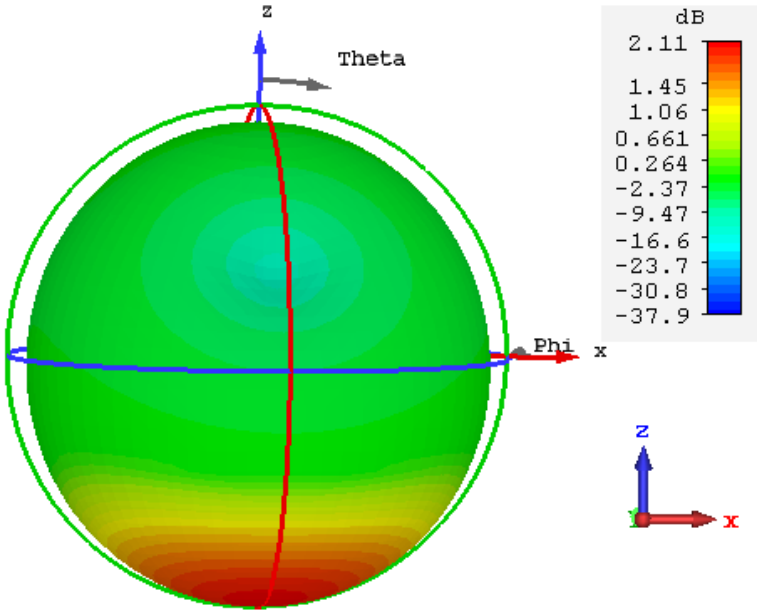

Figure 2.14 Simulated 3D radiation patterns of the proposed Antenna at 5.8 GHz

2.3 Rectangular Concaved Antenna

In order to increase the bandwidth and keeping the simple character of the structure we use concavity for the monopole patch antenna.

2.3.1 Effect of concaving the non-radiating edges of a rectangular monopole antenna

The patch antenna's non radiating edges are curved into an elliptical curvature shape. Only half of the ellipse is overlapped with the patch since it is formed and positioned exactly on the edge of the patch. As illustrated in figure 2.15, the ellipse has a primary axis radius and a secondary axis radius, which is known as the curvature of the patch C.

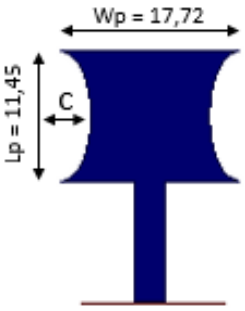

Figure 2.15 Rectangular concaved antenna

The effect of curvature (C) is analyzed as shown in figure 2.16 for the antenna's reflection coefficient. It can be shown that increasing C raises the Structure's resonant frequency and the bandwidth. This rise in the resonance frequency is due to a reduction in the patch's resonant length, which shortens the current path. For C =1.6 mm the first resonant is at 3.565 GHz and the second resonance is at 5.825 GHz. The percent bandwidth of the antenna with the chosen value of C is: $BW\ (\%) = \frac{7.093-2.973}{7.093+2.973} \times 200 = 81.86\%$, indicating a small increase in the bandwidth as compared to the conventional rectangular monopole.

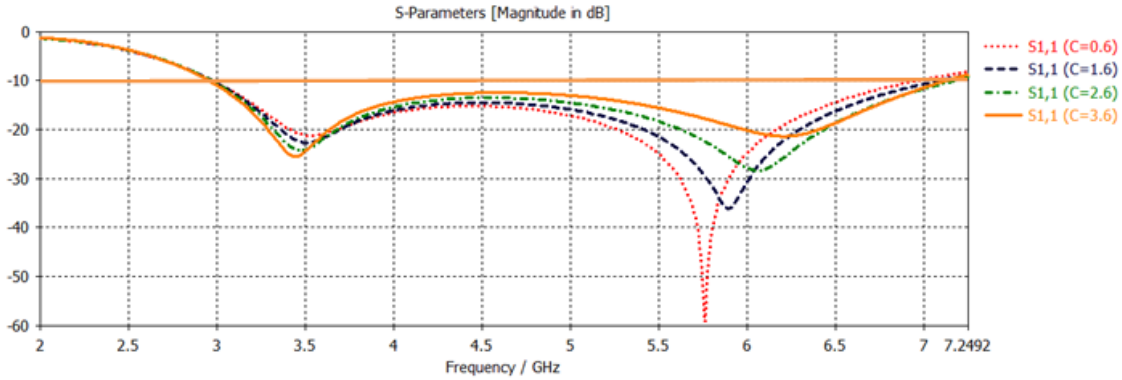

Figure 2.16 Input reflection coefficient of the rectangular patch versus frequency for different values of the curvature C

2.3.2 Input Impedance:

The simulated input impedance of the rectangular monopole patch antenna is shown in figure 2.17. The input impedance of the monopole antenna shows that the structure resonates at 3.565 GHz with a real part of 52.77 Ω and imaginary part of -7.40 Ω. The second mode is appeared at 5.825 GHz with a real part of 53.29 Ω and imaginary part of -1.00 Ω ;which are close to the line impedance (50 Ω) and this ensures a good matching with the feed line and a proper working of the antenna;

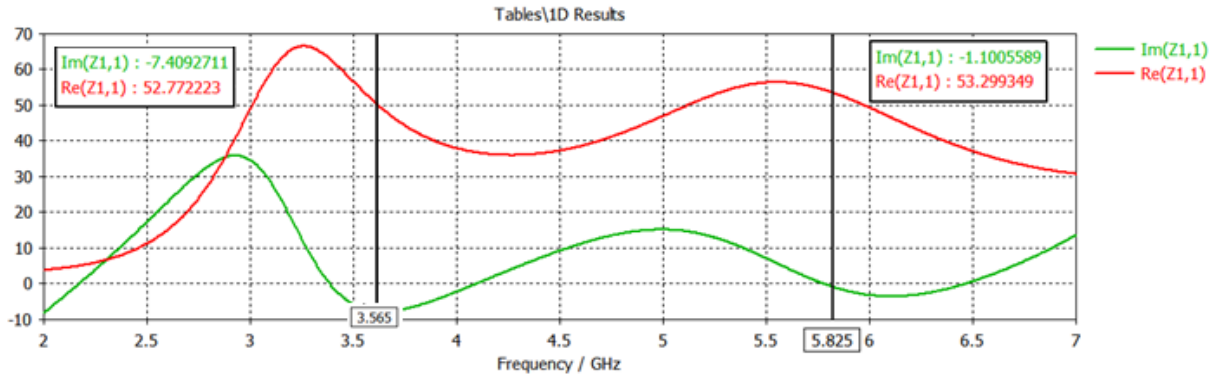

Figure 2.17 Simulated input impedance for monopole patch Antenna

2.3.3 Current distribution

The current pattern around the first resonance at 3.565 GHz is shown in Figure 2.18(a). Figure 2.18(b) shows the current pattern around the second resonance at 5.825 GHz, which indicates a second order harmonic.

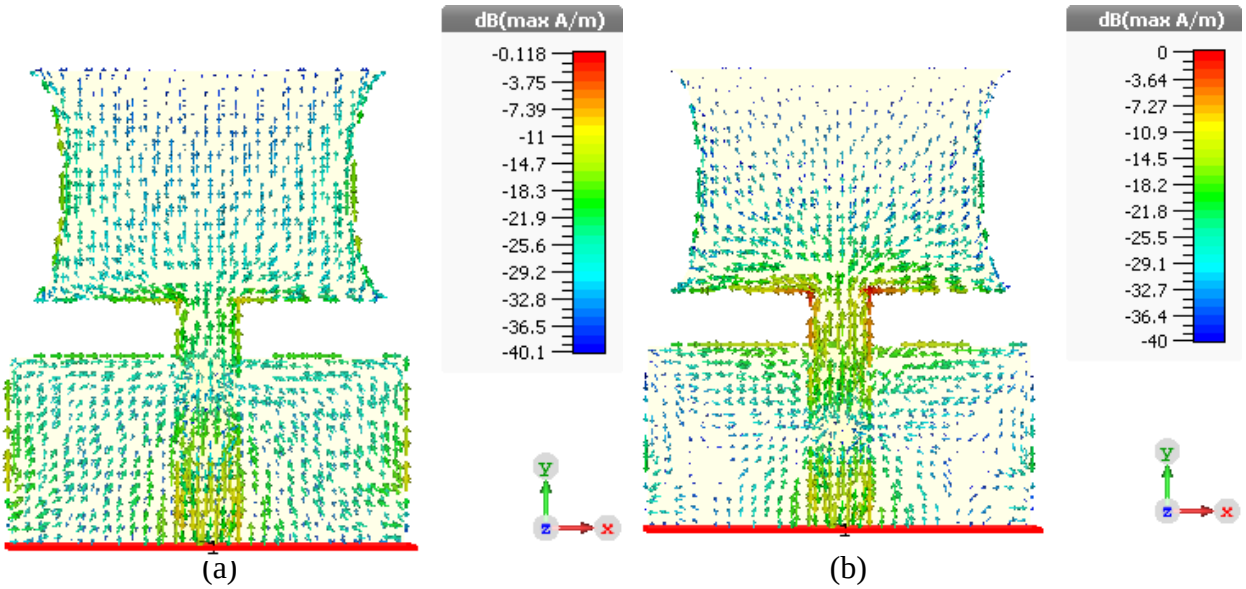

(a) (b)

Figure 2.18 The current distribution of the monopole antenna at (a) 3.565GHz, (b) 5.825GHz

It can be seen that the concentration of surface current is high at the center of concave in the patch.

2.3.4 Radiation Pattern

i) 2D representation of Radiation pattern

Figures 2.19, 2.20, 2.21 and 2.22 illustrate simulated 2D representations of far field radiation patterns at 3.565 GHz and 5.825 GHz respectively. Both co-polar and cross-polar components of the radiated field are drawn in the main planes, E plane and H plane, to examine polarization purity.

Figure 2.18 and Figure 2.19 show that at the 3.565 GHz, the co-polar component is similar the dipole like patterns with a realized gain is 2.01 dB in the E-plane and 1.83 dB in the H-plane; almost the same as the rectangular monopole. The structure also shows very good polarization purity with cross-polar component level of $-89.11\ dB$. However, in the H-plane, the cross-polar component is only – 14.43 dB lower than the co-polar.

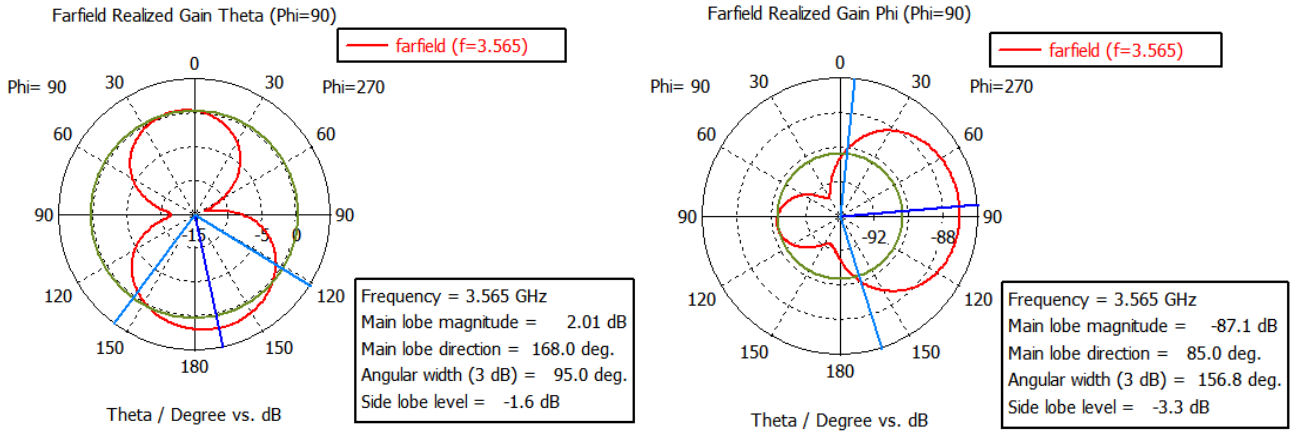

Figure 2.19 E-plane radiation field pattern of the monopole antenna at 3.565 GHz
(a) co-polar , (b) cross-polar

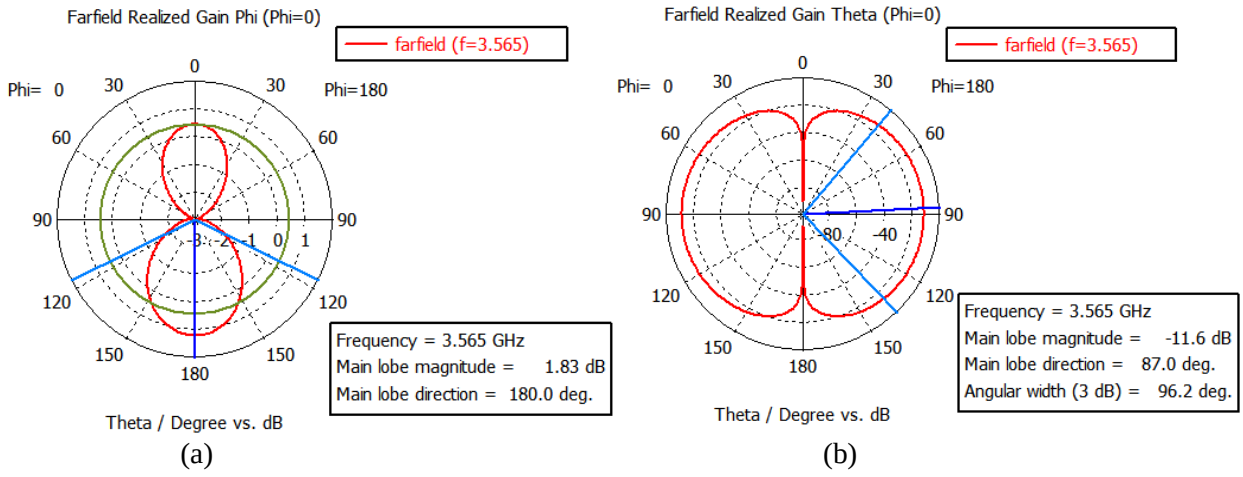

Figure 2.20 H-plane radiation field pattern of the monopole antenna at 3.565 GHz
(a) co-polar , (b) cross-polar

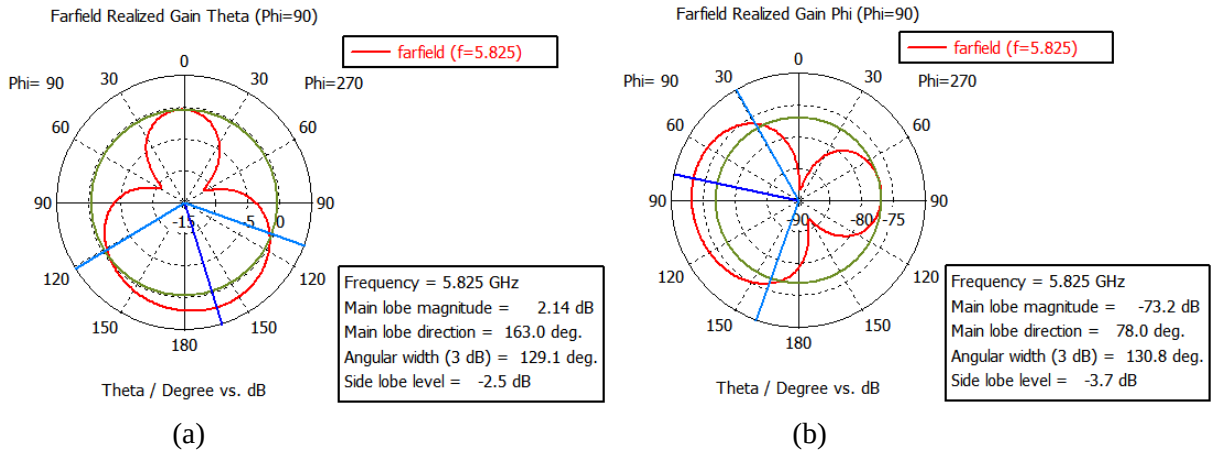

Figure 2.21 E-plane radiation field pattern of the monopole antenna at 5.825 GHz
(a) co-polar , (b) cross-polar

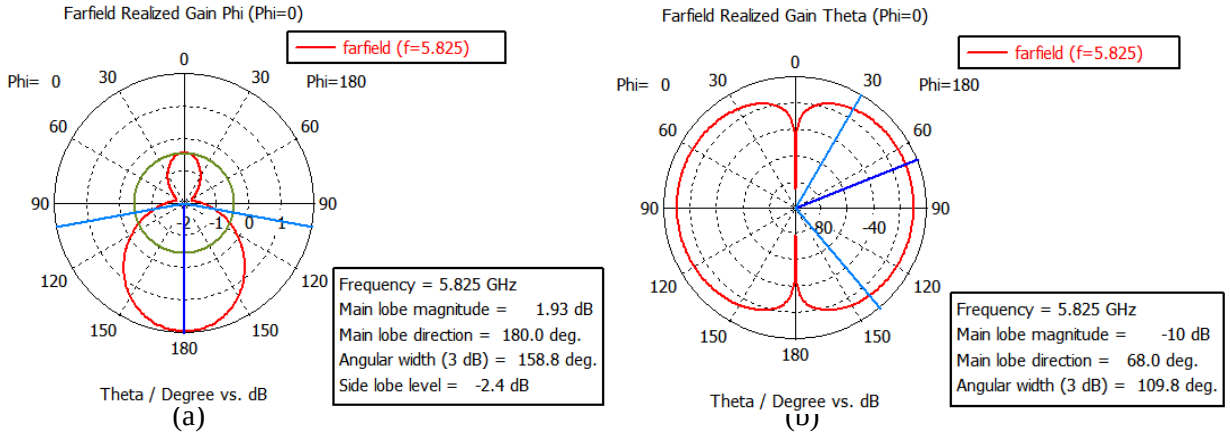

Figure 2.22 H-plane radiation field pattern of the monopole antenna at 5.825 GHz
(a) co-polar , (b) cross-polar

At the 5.825 GHz, the fields are shown in Figure 2.20 and Figure 2.21; the E-plane and the H-plane respectively. In the E-plane, the co-polar component is quite pinched with realized gain is 2.14 dB and the cross-polar component with a level $-75.34\ dB$ lower than the co-polar indicates good polarization purity. For the H-plane, the co-polar component shows that the field is mainly directed toward the 180° with a gain of 1.93 dB while the cross-polar is $-11.93\ dB$ lower than the co-polar. These results indicate that the two monopoles have almost the same characteristics.

2.4 Conclusion

In this chapter the rectangular and concaved rectangular monopoles are designed and behave as UWB structures. It is found that the bandwidth of the concaved monopole is increased as compared to the rectangular one.

CHAPTER 3

Rectangular MIMO Antenna with concavity and isolation

CHAPTER 3: Rectangular MIMO Antenna with concavity and isolation

3.1 Introduction

This chapter proposes a technique for reducing mutual coupling in MIMO system. This solution is based on the use of concavity in the non-radiating edges of the patches and adding isolation between the two patches.

3.2 Rectangular MIMO Antenna

The geometry of the proposed UWB MIMO antenna is shown in Figure 3.1. A planar rectangular shaped antenna is designed with a size of Wp = 17.72mm, Lp = 11.45mm. The antenna consists of two symmetrical rectangular planar-monopole antenna elements. The two antenna elements are placed in parallel with each other and fed through a microstrip feed line. Before performing the study of this structure, the effect of the distance between both antennas -d-is analysed for achieving minimum mutual coupling with low reflection coefficient that conserve the UWB frequency standard.

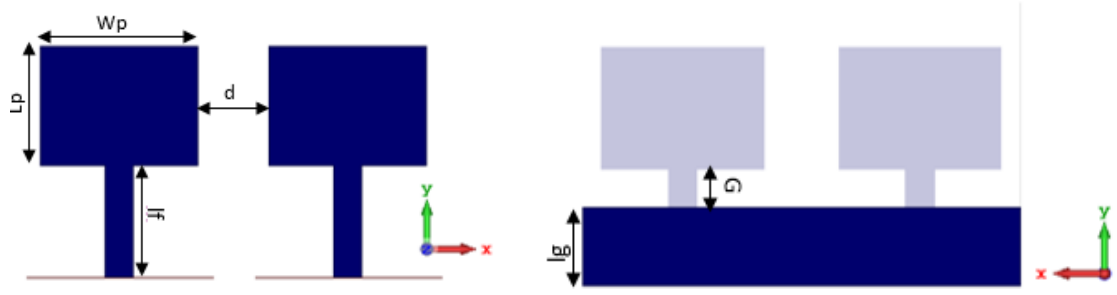

(a) (b)

Figure 3.1 Rectangular MIMO antenna. (a) Front view, (b) Back view

3.2.1 Effect of the gap spacing

The reflection coefficients of the MIMO antenna with different values of the separation distance are illustrated Figure 3.2. From this figure, it is noticed that the decrease in the gap spacing -d- results in the decrease of the first resonant frequency and the increase in the second one. However, the increase in this parameter above 8mm the structure operates as a singlewide band antenna since the coupling starts to disappear. So, this value of d seems to be

the best that offers ultra wide bandwidth with satisfactory matching and important mutual coupling should be reduced.

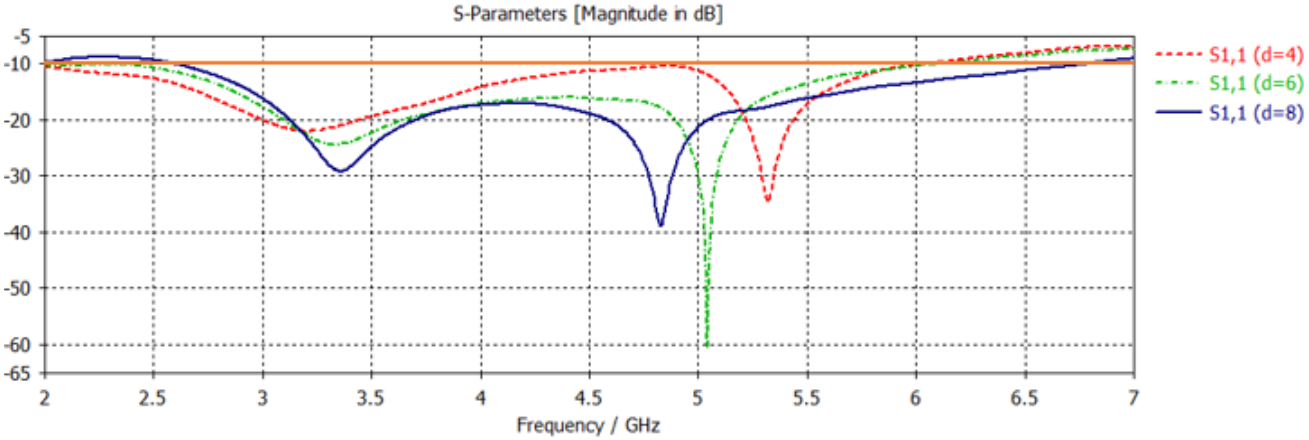

Figure 3.2 The effect of the gap spacing on the input reflection coefficient

3.2.2 The input reflection coefficient

The input reflection coefficient of the rectangular MIMO antenna is plotted in Figure 3.3.It is observed that the Antenna is working from 2.6 to 6.77 GHz. From this figure, the frequency bandwidth using the frequencies at -10 dB is obtained as:

$$\mathrm{BW}(\%) = 200 \times \frac{6.77-2.60}{6.77+2.60} = 90.65\%$$

This value indicates clearly that the considered structure is an UWB structure.

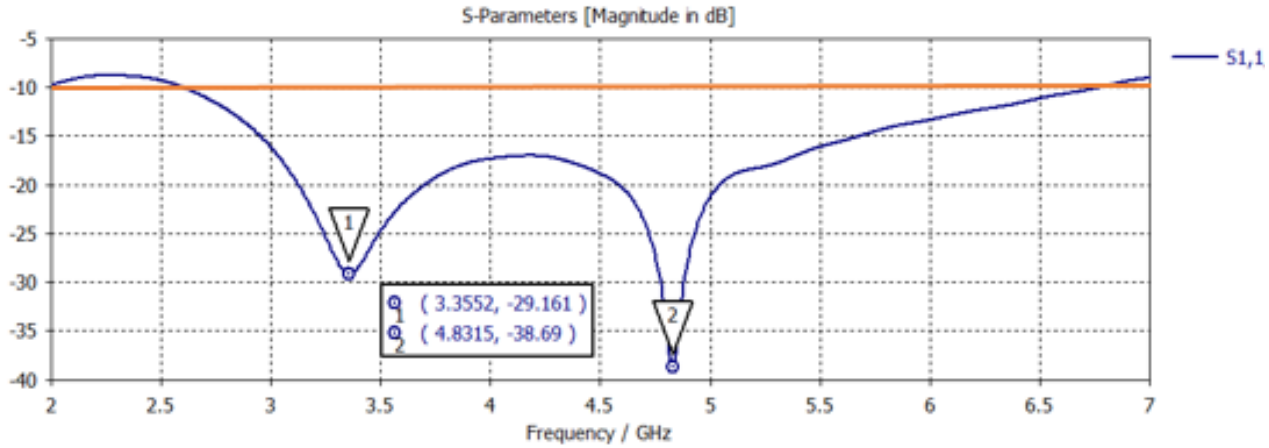

Figure 3.3 The input reflection coefficient of the rectangular MIMO antenna

3.2.3 Mutual coupling

The mutual coupling between the elements in the MIMO antenna is an important parameter and related to antenna efficiency for such system. The higher value of the mutual coupling degrades the antenna efficiency and in this antenna the mutual coupling is observed from S21

parameter as illustrated in figure 3.4.The figure shows that the mutual coupling is higher than $-15d$, which is within unaccepted range. To overcome this, an isolator will be added to the ground between the two patches, leading to the decrease of the mutual coupling.

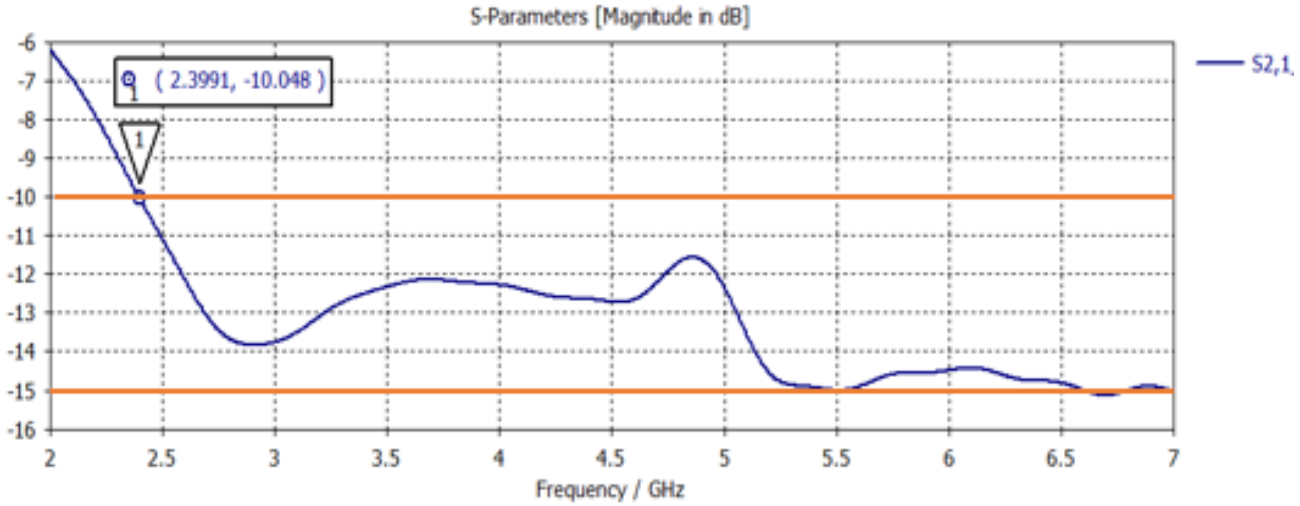

Figure 3.4 The mutual coupling of the rectangular MIMO antenna

3.3 Rectangular MIMO Antenna with Isolator

To enhance isolation between the antennas, a rectangular isolator is placed between the antenna elements as depicted in figure 3.5. The isolator diverts the surface currents so that the mutual coupling is reduced and isolations is increased.

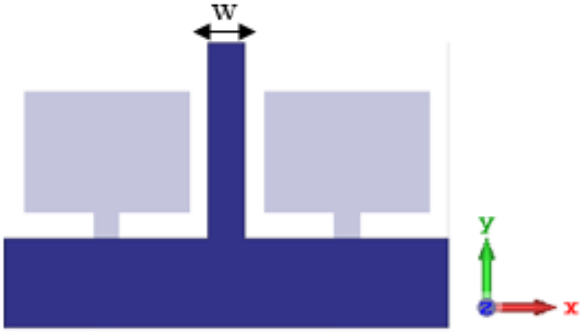

Figure 3.5 The isolation of the rectangular MIMO antenna

3.3.1 Effect of the width of the isolator

Figure 3.6 shows the mutual coupling curves with different values of the width of the isolator. First, it is noticed that the insertion of the metallic wall results in the decrease of the coupling between the MIMO elements. Second, by increasing the width of the isolator, the mutual coupling decreases. However, a further increase in this width leads to a inverse effect since

the monopole character of the structure will be lost. So, an educated study of this parameter is needed in case a special application of such system is required.

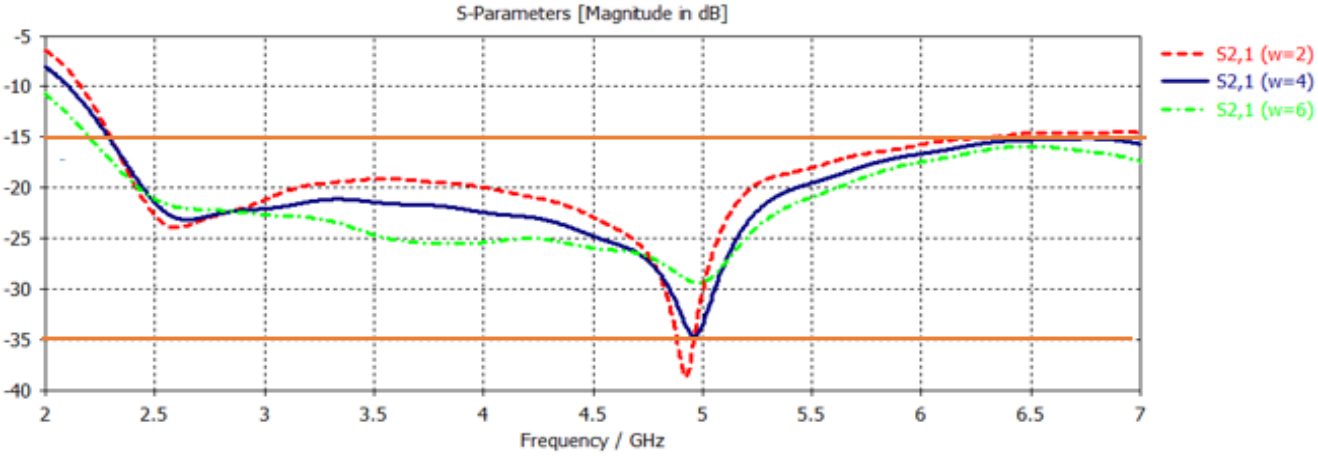

Figure 3.6 The effect of the width of the isolator on the mutual coupling of the MIMO Antenna

3.3.2 The input reflection coefficient

The structure of MIMO system with rectangular isolator is shown in figure 3.5. The separation distance between the two patches is 8mm, and the isolator width is fixed to 4 mm with keeping the same length and width of the two patches as mentioned before. After simulating the resulted structure, the input reflection coefficient of a patch is illustrated in figure 3.7. The figure indicates clearly that the structure behave almost the same as a rectangular monopole alone.

The structure behaves an UWB structure with a percent bandwidth of about:

$$BW = 200 \times \frac{6.61-2.29}{6.61+2.29} = 97.08\%;$$

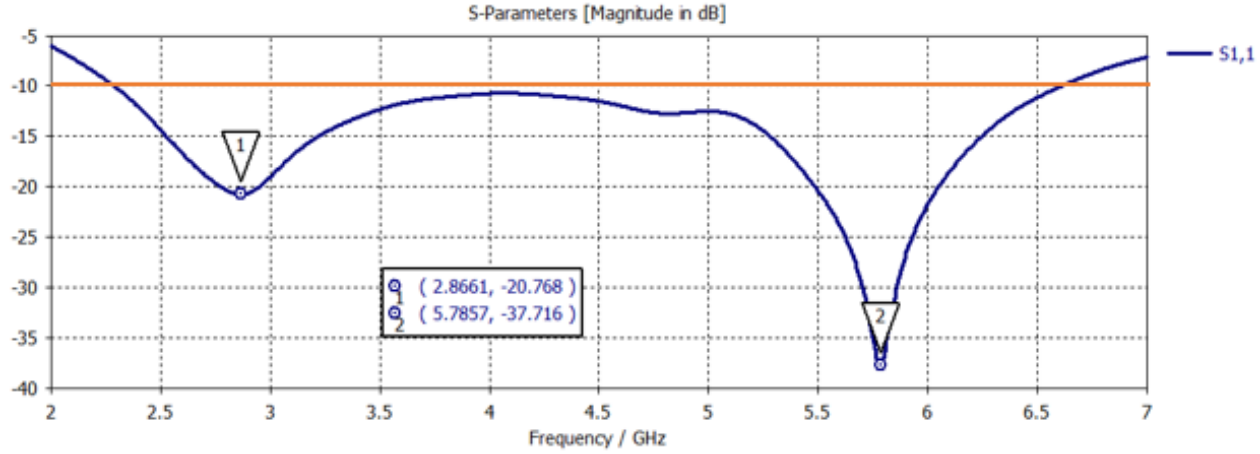

Figure 3.7 The input reflection coefficient of the rectangular MIMO antenna with isolator

A comparison between the MIMO and Monopole antenna without concavity is given in table 3.1:

Table 3.1. Comparison between the MIMO antenna and Monopole without concavity

	Start frequency	**Ending frequency**	**bandwidth**	**First resonant frequency and S_{11} level**	**second resonant frequency and S_{11} level**
Monopole antenna	2.96 GHz	6.96 GHz	80.50%	3.5 GHz -22.12 dB	5.8 GHz -48.01 dB
MIMO Antenna	2.29 GHz	6.61 GHz	97.08%	2.86 GHz -20.77 dB	5.78 GHz -37.72 dB

For further decrease in the mutual coupling a concavity is introduced in non-radiating edges of the patches. The effect of the concavity "C" is studied in the previous chapter.

3.4 The rectangular MIMO antenna with concavity and isolator

Since the concavity decreases the mutual coupling between microstrip radiating patches [28], and rectangular isolator enhance isolation between the ports, a rectangular concaved MIMO antenna with isolator is designed, as shown in figure 3.8, using the same dimensions of the antenna mentioned in the previous chapter.

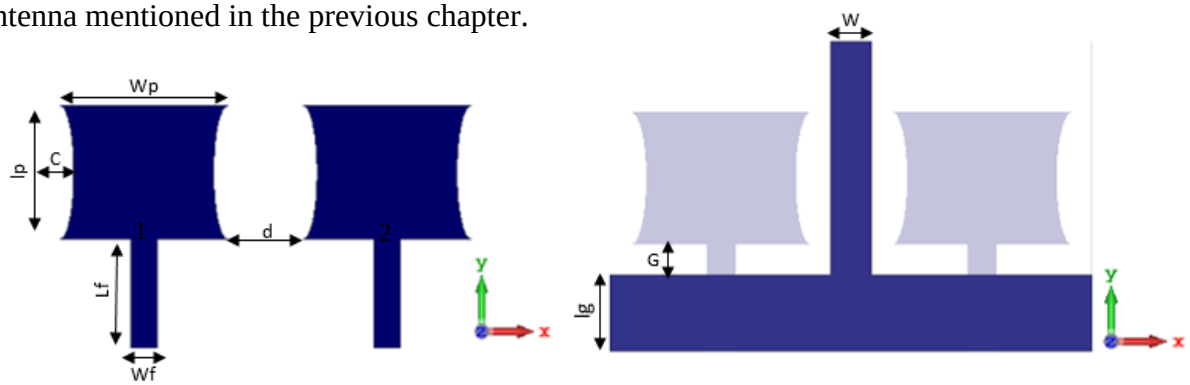

(a) (b)

Figure 3.8 The rectangular MIMO antenna with concavity and isolator, (a)front, (b)back

Table 3.2. Dimensions of the proposed antenna in (mm)

Parameters	ws=wg	Ls	lg	wp	Lp	Wf	Lf	G(gap)	C	w	d
Dimensions	47.4	30.5	9.5	17.72	11.45	3.08	12.5	3	1.6	4	8

3.4.1 Results and discussions

3.4.1.1 The input reflection coefficient

The input reflection coefficient of the proposed structure is presented in Figure 3.9. Again, the structure behaves an UWB structure with a percent bandwidth of about:

$BW = 200 \times \frac{6.50-2.64}{6.50+2.64} = 84.46\%$;

Accordingly, the bandwidth of this structure is reduced as compared with the rectangular MIMO inversely with the isolated monopole.

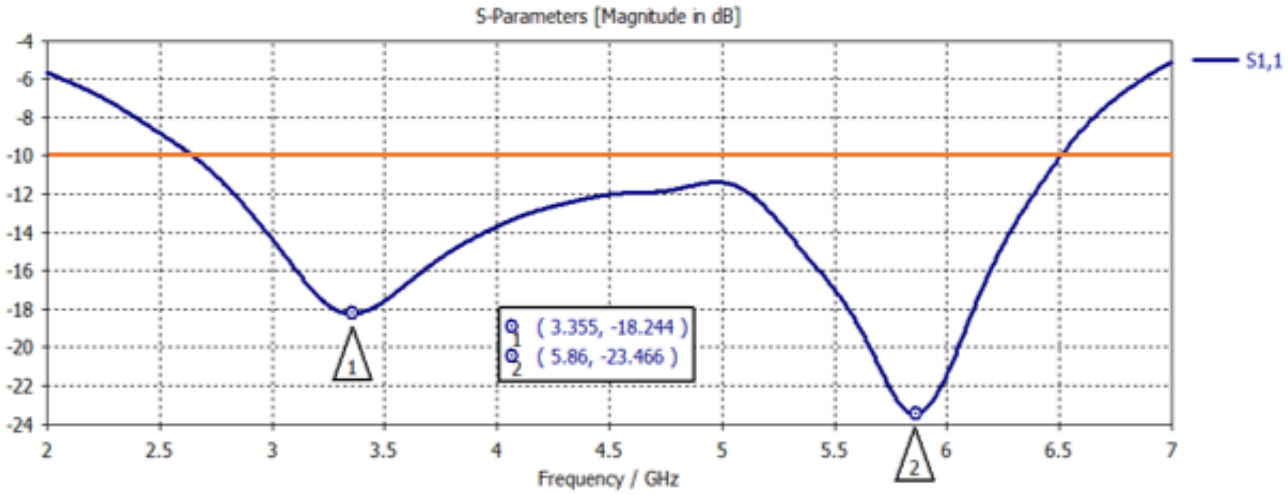

Figure 3.9 The input reflection coefficient of the concaved MIMO Antenna

A comparison between the MIMO antenna and Monopole with concavity is given in table 3.3:

Table 3.3. Comparison between the MIMO antenna and Monopole with concavity

	Start frequency	**Ending frequency**	**bandwidth**	**First resonant frequency and S_{11} level**	**Second resonant frequency and S_{11} level**
Monopole antenna	2.97 GHz	7.09 GHz	81.86%	3.56 GHz -22.5 dB	5.82 GHz -35 dB
MIMO Antenna	2.64 GHz	6.50 GHz	84.46%	3.35 GHz -18.24 dB	5.86 GHz -23.46 dB

3.4.1.2 The mutual coupling

The mutual coupling of the rectangular MIMO Antenna and the one with concavity are drawn in the same figure for purpose of comparison as shown in figure 3.10. It is clearly noticed that the introduced concavity results in lowering the mutual coupling between the elements of the MIMO structure.

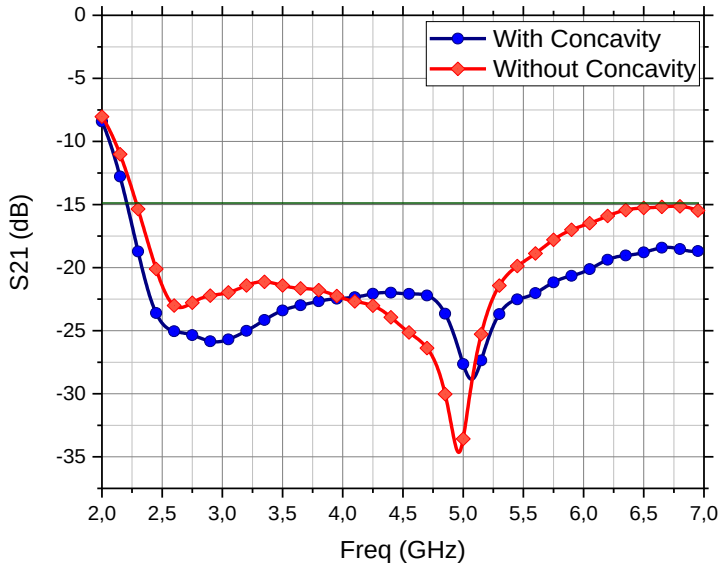

Figure 3.10 The comparison between the results of S21 of the two MIMO antennas

3.4.1.3 The current distribution

The current patterns of port one and two are shown in figures 3.11 and 3.12 respectively around the first and second resonance frequencies. The figures 3.11 and 3.12 indicate that the isolator blocs currents coming from the excited patches especially at the lower frequencies within the operating bandwidth. However, as we increase in the frequency, the structure tends to operate in the higher order modes leading to less coupling (apparent in the isolator with more currents as compared the lower frequency case). This may necessitate other technique of reducing mutual coupling at higher frequencies with the band.

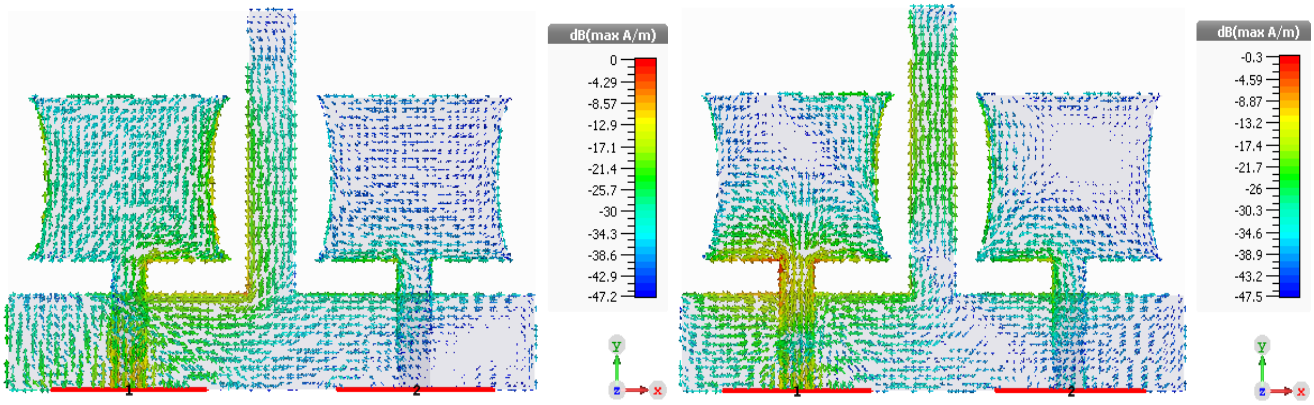

(a) (b)

Figure 3.11 The current distribution of port 1. (a)3.355GHz, (b)5.86Ghz

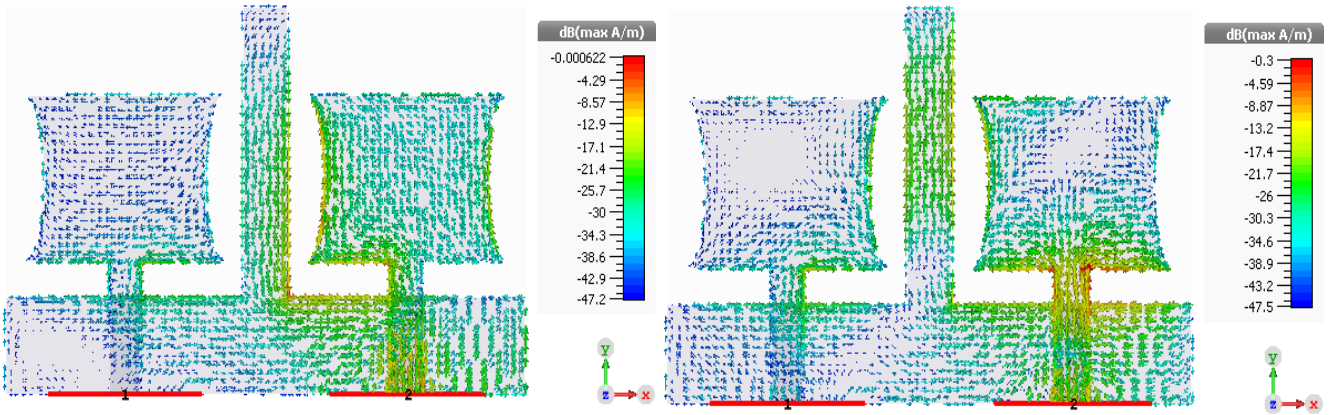

(a) (b)

Figure 3.12 The current distribution of port 2. (a)3.355GHz, (b)5.86Ghz

3.4.1.4 The radiation pattern

The radiation patterns of the proposed antenna system are investigated in the operating frequency range of 2.64-6.5 GHz. The study of the antenna pattern have been observed in the

electric field in both planes E-plane and H-plane at the two frequencies 3.355 GHz and 5.86 GHz as shown in figures below.

It is noticed that, in the two planes the level of the cross polar components is quite high. This is attributed to the isolator that reacts as an antenna with a principle current orthogonal to copolar current. Also we notice that, depending on wich port we excite, the radiated field maximum radiation direction is deflected in the direction opposite to the isolator. Further more, the patterns are almost omnidirectional with deflected direction at lower resonance, and become distorted at the higher harmonic.

To overcome the problem of deflection of the radiated field from each monopole due to the isolator we suggest addition of another isolator on the top of the dielctric material. This will create a capacitive effect that absorbs the field instead of radiating it. But we expect a change in the frequency band of operation that may be adjusted by varying patch dimensions and separation between the MIMO antenna elements.

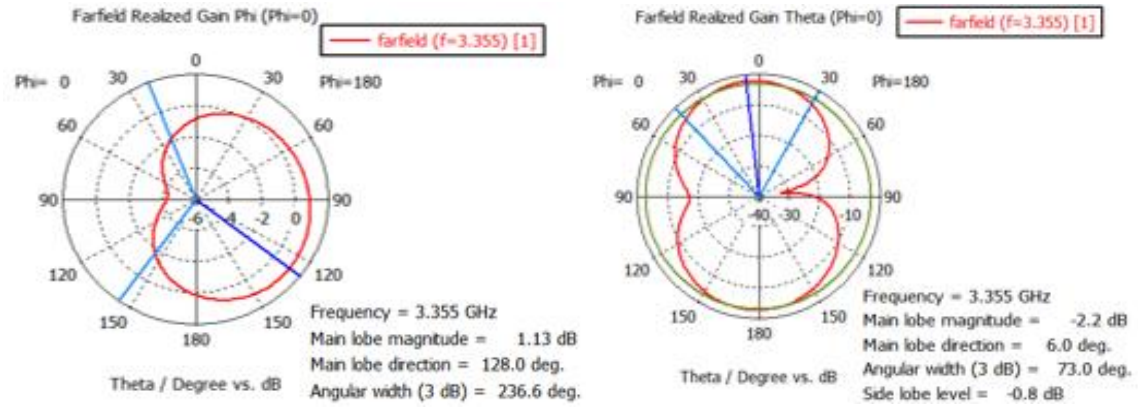

(a) (b)

Figure 3.13 H-plane radiation field pattern of the MIMO antenna of port 1 at 3.355GHz (a) co-polar, (b) cross-polar

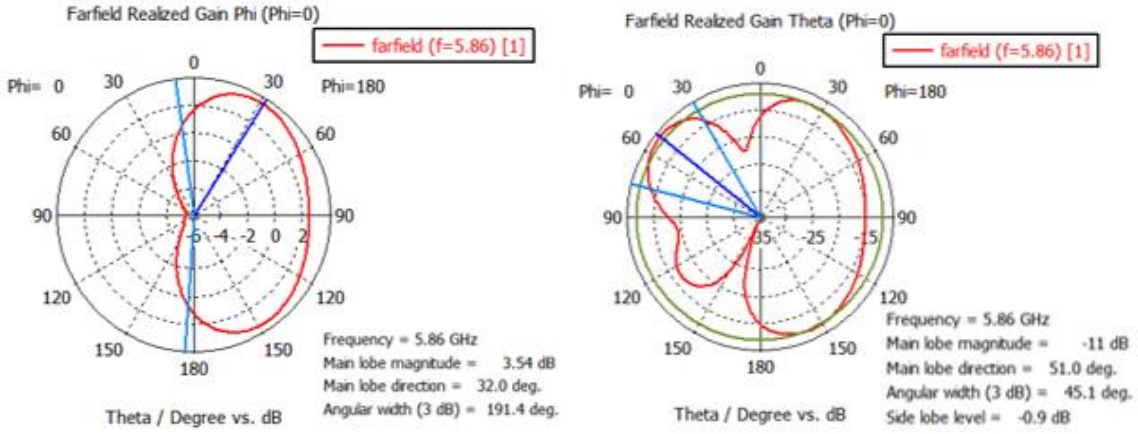

(a) (b)

Figure 3.14 H-plane radiation field pattern of the MIMO antenna of port 1 at 5.86GHz (a) co-polar, (b) cross-polar

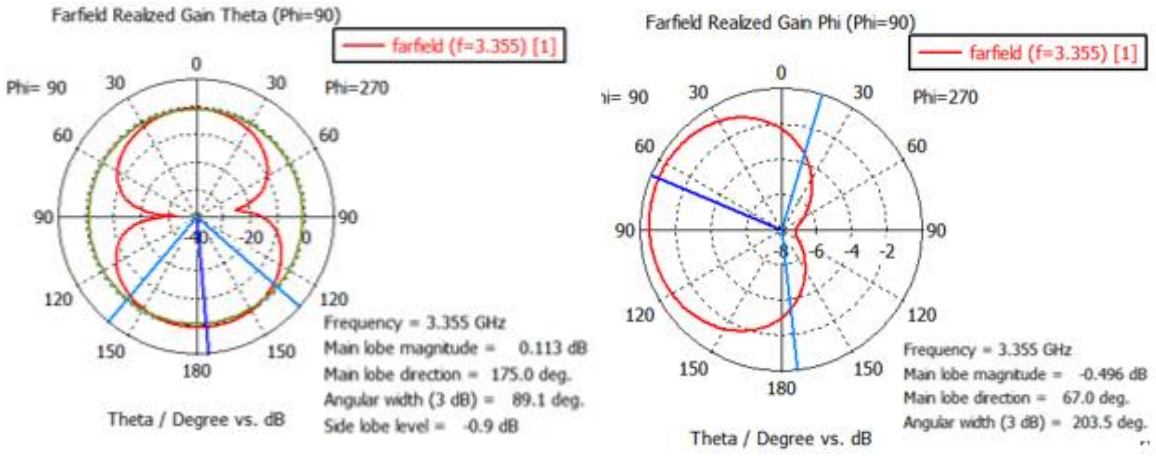

(a) (b)

Figure 3.15 E-plane radiation field pattern of the MIMO antenna of port 1 at 3.355GHz (a) co-polar, (b) cross-polar

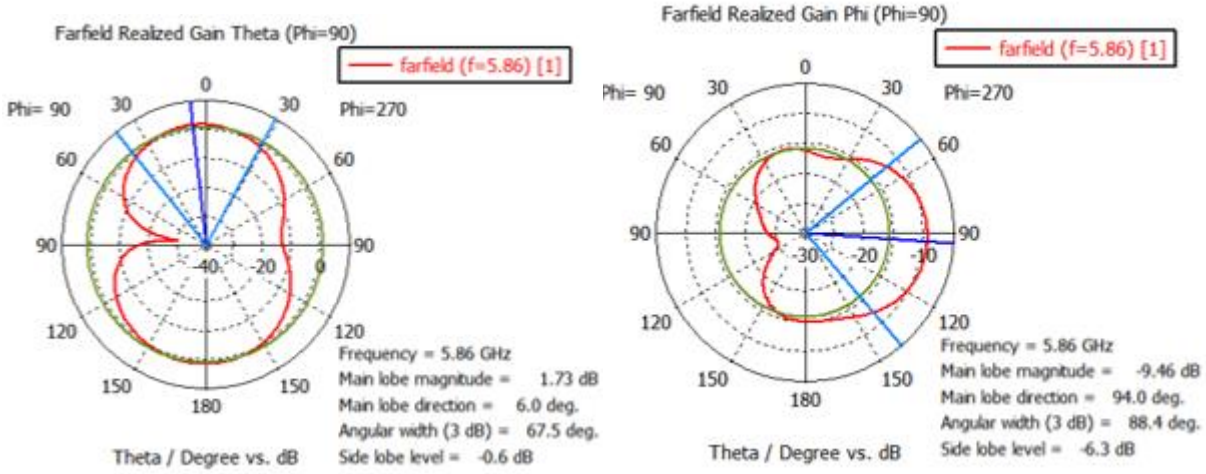

(a) (b)

Figure 3.16 E-plane radiation field pattern of the MIMO antenna of port 1 at 5.86GHz (a) co-polar, (b) cross-polar

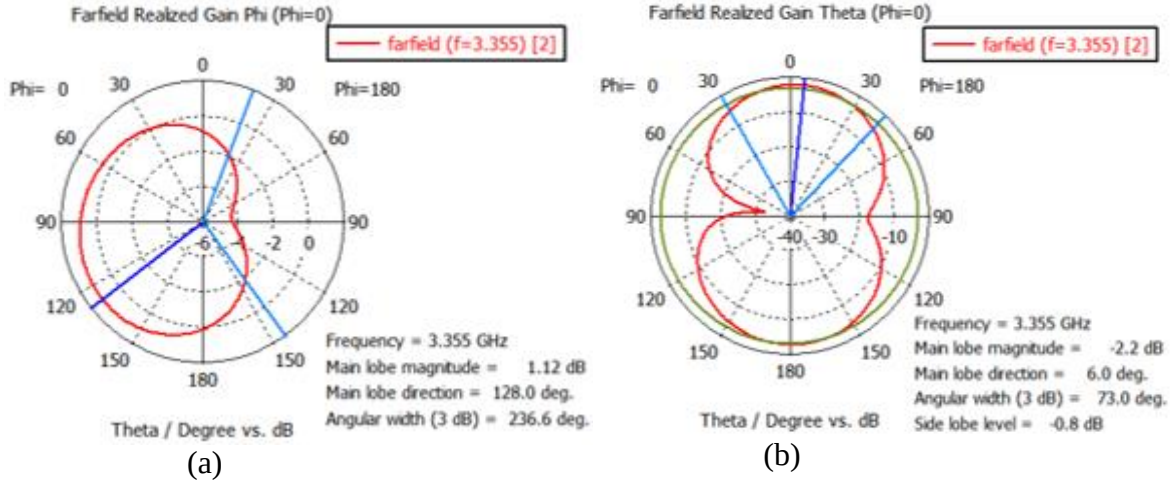

(a) (b)

Figure 3.17 H-plane radiation field pattern of the MIMO antenna of port 2at 3.355GHz (a) co-polar, (b) cross-polar

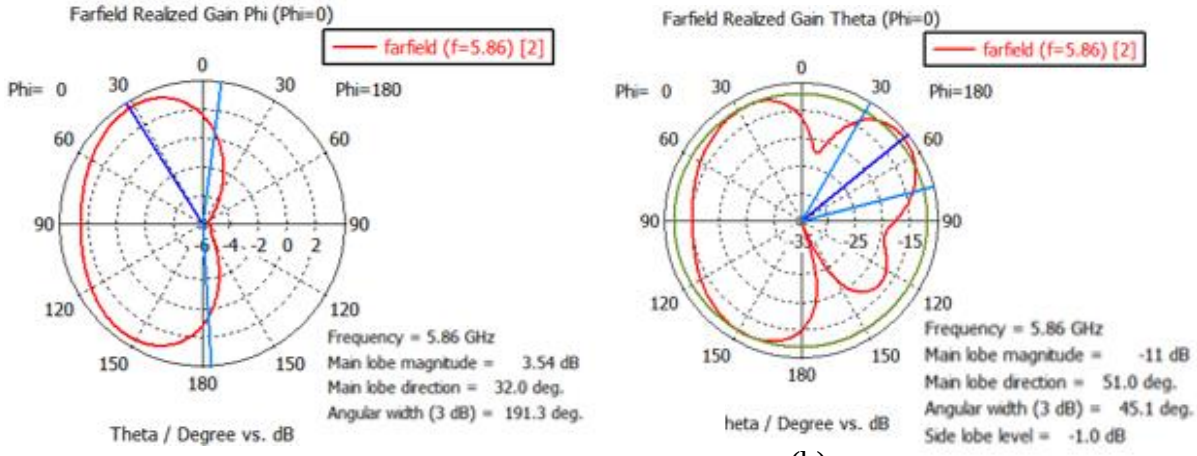

(a) (b)

Figure 3.18 H-plane radiation field pattern of the MIMO antenna of port 2 at 5.86GHz (a) co-polar, (b) cross-polar

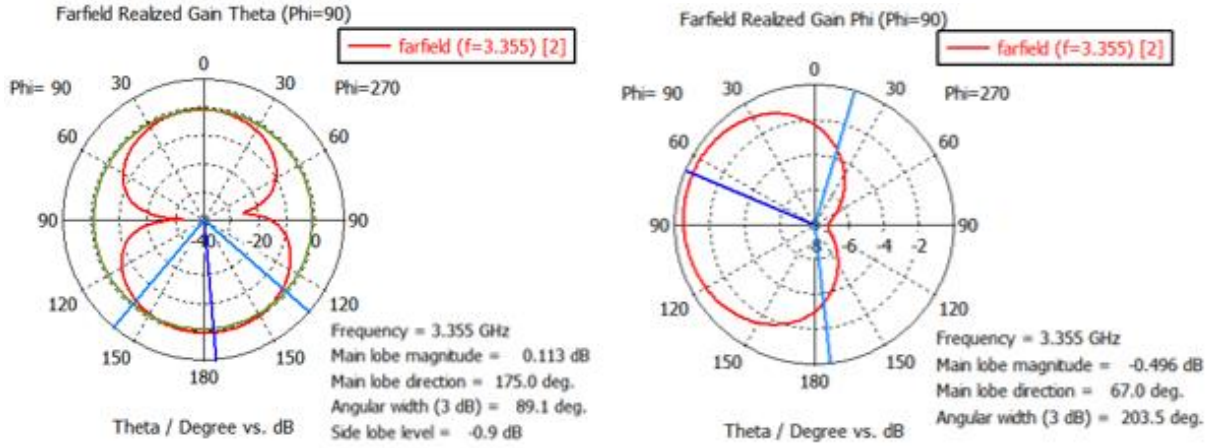

(a) (b)

Figure 3.19 E-plane radiation field pattern of the MIMO antenna of port 2 at 3.355GHz (a) co-polar, (b) cross-polar

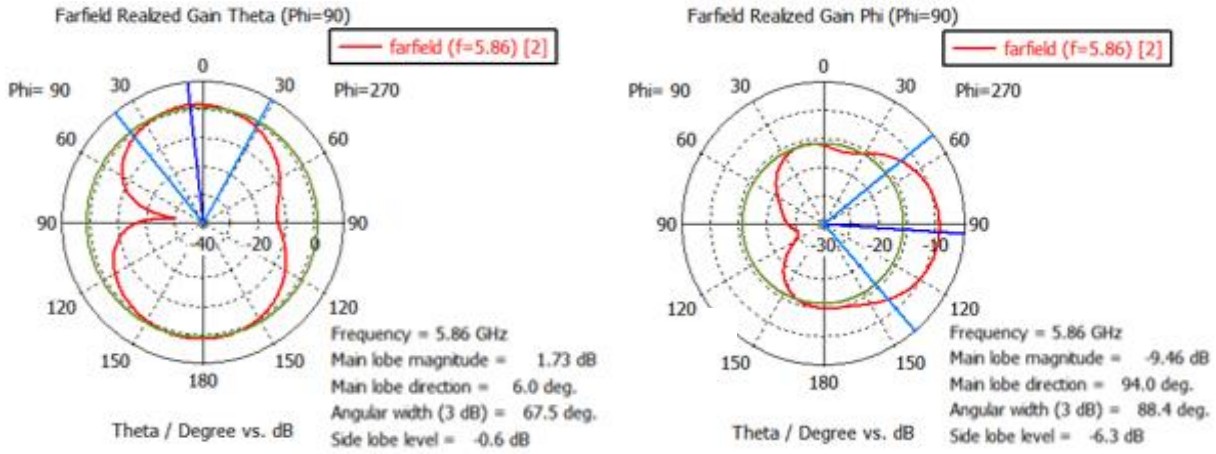

(a) (b)

Figure 3.20 E-plane radiation field pattern of the MIMO antenna of port 2 at 5.86GHz (a) co-polar, (b) cross-polar

3.5 Realization and Measurements

To confirm the simulation results obtained previously, the final structure is realized using the available PCB prototyping machine "MITS ELECTRONICS" shown in Figure 3.21.

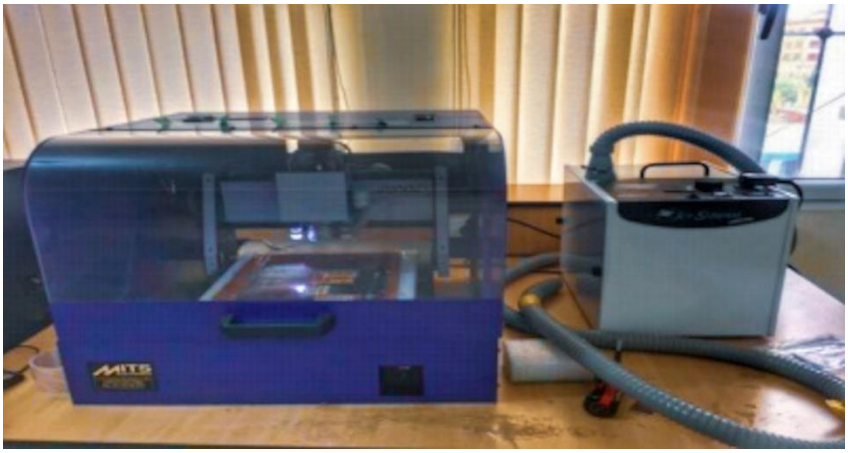

Figure 3.21 The PCB prototyping machine

The constructed antenna is shown in Figure 3.22.

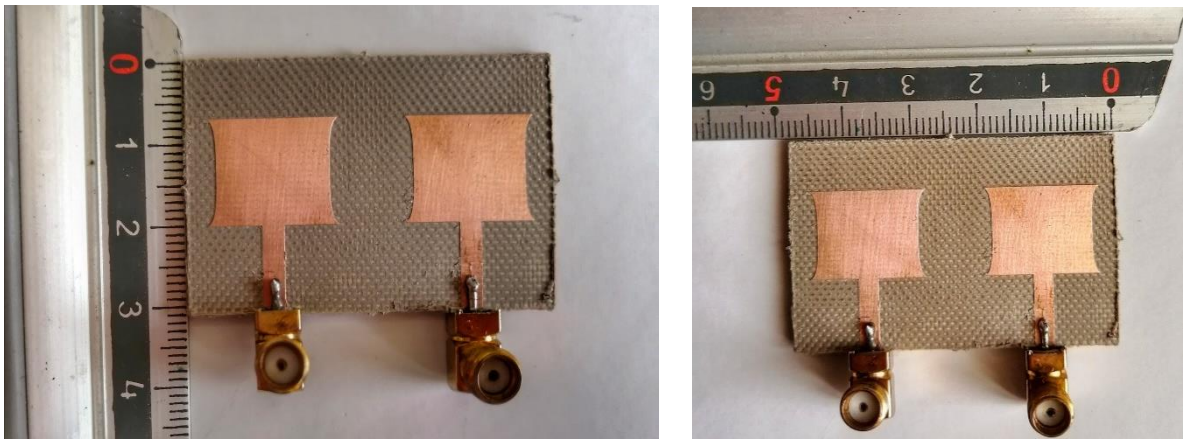

(a)

(b)

Figure 3.22 Realized MIMO antenna (a) patches, (b) ground

The measurement of the input reflection coefficient is carried out using the vector network analyzer shown in Figure 3.23.

Figure 3.23 Vector Network Analyzer used for measurement

The measured input reflection coefficient and the mutual coupling of the MIMO antenna together with the simulated results are shown in Figure 3.24 and 3.25 respectively. The measured results confirm the UWB behavior of the structure with reduced coupling between the elements of the MIMO Antenna. A comparison between measured results and simulations show acceptable level of agreement between but with small deviations. This is due to the fact that the FR4 dielectric is not appropriate to frequencies above 4 GHz, incertitude in its parameters, the tolerance in fabrication and soldering and the measurement environment which contains the reflecting obstacles.

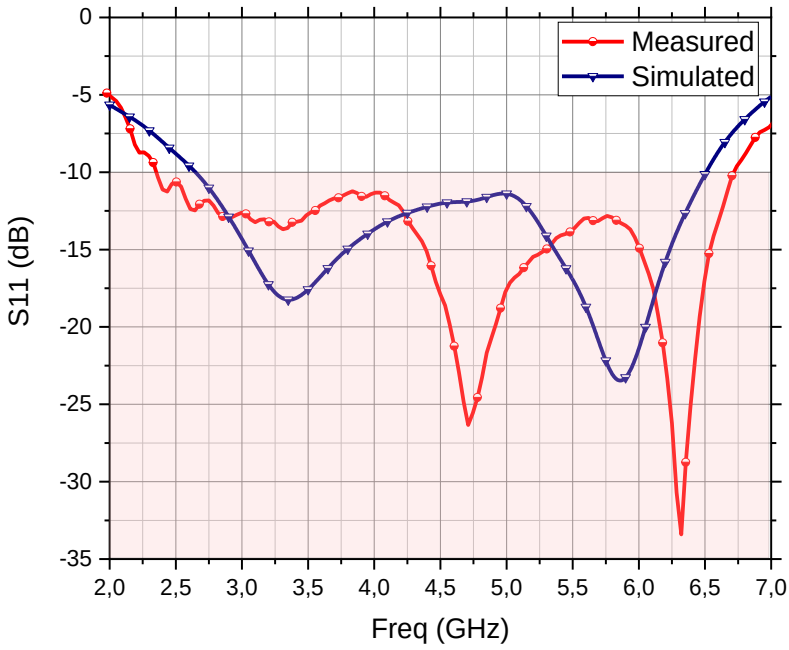

Figure 3.24 Measured and simulated input reflection coefficient of the MIMO Antenna

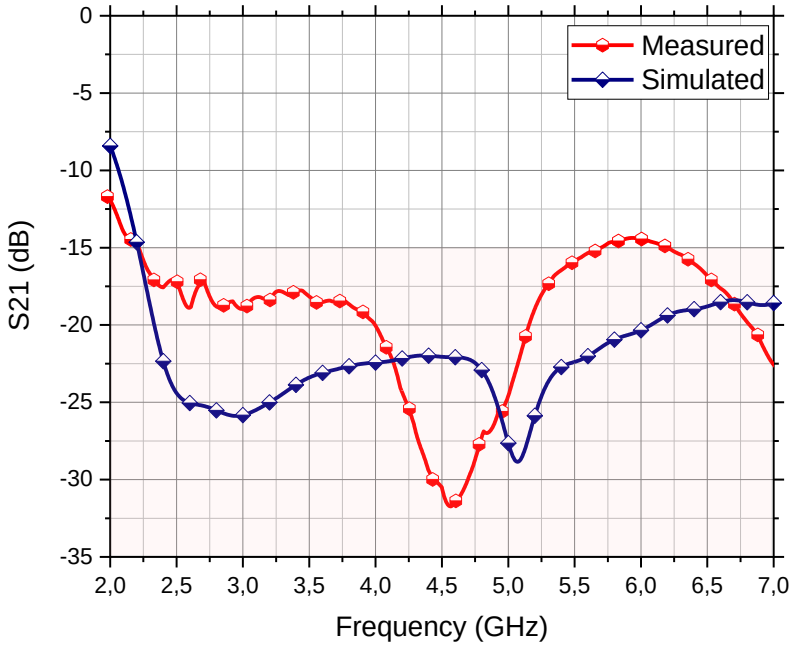

Figure 3.25 Measured and simulated mutual coupling of the MIMO Antenna

A quantitative comparison between measured and simulated input reflection coefficient of the concaved MIMO antenna is summarized in Table 3.4.

Table 3.4 comparison between measured and simulated input reflection coefficient of the concaved MIMO antenna

	Start Frequency	Ending frequency	Bandwidth %
Simulated	2.64 GHz	6.50 GHz	84.46%
Measured	2.30 GHz	6.75GHz	98.34%
Error %	34%	25%	13.88%

3.6 Conclusion

In this chapter, UWB MIMO antennas in the form of rectangular and concaved rectangular are studied. A technique for reducing the mutual coupling is applied in both structures. The results for the concaved structure are confirmed by practical implementation and measurement.

General Conclusion

In this report, theoretical as well as practical aspects of UWB technology for UWB monopole antenna and MIMO antenna are investigated and established systematically. Five UWB antennas with enhanced bandwidth are specifically scrutinized through varied simulations and measurements. These include rectangular with and without concavity UWB monopole antenna, rectangular MIMO UWB antenna, rectangular MIMO UWB antenna with isolator and rectangular MIMO UWB antenna with concavity and isolator.

The evolution steps of the designed antennas are evaluated to have an insight into their ultra wide band nature. Initially, the designed antennas are investigated by the simulation studies of various parameters in terms of reflection coefficient and mutual coupling. Finally, the designs are validated by fabrication and measurements.

It shown that an introduction of concavity in the non-radiating edges of the rectangular monopole increase the bandwidth with almost the same far zone fields for the two structures. These two monopoles are arranged in the MIMO structure with two elements. The simulations of the resulted MIMO antennas present an important coupling between their elements. To minimize this coupling, an isolator in the form of rectangular strip, with a suitable width, is etched in the ground side between the two monopoles. The simulation results proved the usefulness of this technique in the mutual coupling reduction (below -15 dB) but in the expense of radiation patterns (shift of the main beam in the E-plane and high level of the cross-polarization component in the H-plane).

To validate the simulation results, the concaved MIMO structure is fabricated on the FR4 dielectric substrate. The measurements of the input reflection and the transmission coefficients present agreement with simulations within the limits of measurement conditions.

This work may be further extended and improved by doing the following tasks:

- Use an extra strip coplanar with the patch to compensate for the field deviation by creating a capacitive effect
- Increase the bandwidth of the antennas by introducing defects in appropriate places on the patch;
- Use other forms of the radiating antennas for improved performances;
- Use other technique for mutual coupling reduction

References

[1] C. A.Balanis, Antenna Theory Analysis And Design -3rd Edition, New Jersey: John Wiley & Sons, 2016.

[2] B. D. PATEL, «"Microstrip Patch Antenna- A Historical Perspective of the Development" Conference on Advances in Communication and Control Systems,» (CAC2S 2013), H. O. D, E. T Department, College Of Engineering Roorkee, Roorkee, U.A-247667, india, 2013.

[3] B. Tharini, "DESIGN OF AN ASSCHERSHAPED MONOPOLE UWB ANTENNA" , ICTACT JOURNAL ON MICROELECTRONICS, JULY 2019

[4] ANR017 GNSS Antenna Selection version 1.1, JULY31, 2020,

[5] Narinder Sharma, "A Study Of Different Feeding Mechanisms In Microstrip Patch Antenna ",February 2017

[6] S. KECHIR, A .NABTI «Study of Rectangular Microstrip Antenna With Parasitic Element,» Master Project. IEEE,University M'hamed Bougara, Boumerdes,algeria, 2016.

[7] T. S. KESHAV, L. M. V. PARUPALLI, S. CHAKRAVARTY,P. RAMACHANDRAN, On Antenna Design, Simulation and Fabrication, India: 2007, PhD Thesis,Deemed University, Nagpur.

[8] G.KUMAR, K. P. RAY, Book, "Broadband Microstrip Antennas",Artech House, Boston.london, 2003.

[9] M. ZENNIR, M. A .YADJAR , «Analysis of a Microstrip Antenna With a Novel Fractal Shape,» ; Master Project. IEEE/ University M'Hamed BOUGARA, Boumerdes, 2018.

[10] B. JAIN, P. SINGLA, R. R. PRASAD, N. SHARMA, «RECTANGULAR PATCH MICRO STRIP ANTENNA: A SURVEY,» Department of Electronics and Communication, Dronacharya Group of Institutions,Greater Noida, U.P, India, 2014; International Advanced Research Journal in Science, Engineering and Technology.

[11] P. A. Azrar, "Antennas "Fundamental Parameters Of Antennas"," Igee/Umbb ,Boumerdes, Algeria.

[12] Song, Y.; Guo, N.; Qiu, R.C. Towards a real-time UWB MIMO test bed for sensing and communications.Proc. IEEE Southeastcon. 2011, 59–63.

[13] Vuong T.P., Ghiotto A., Duroc Y., Tedjini S. "Design and characteristics of a small Uslotted planar antenna for IR-UWB". Microwave and Optical Technology Let. 2007; 49 (7) 1727-1731.

[14] Ali Imran Najam, Yvan Duroc and Smail Tedjini," Multiple-Input Multiple-Output Antennas for Ultra Wideband Communications", Grenoble Institute of Technology, France

[15] Licul S., Noronha J.A.N., DavisW.A., Sweeney D.G., Anderson C.R., Bielawa, T.M. A parametric study of time-domain characteristics of possible UWB antenna architectures. Proceedings of IEEE 58th Vehicular Technology Conf., Vol. 5, (3110-3114), Oct. 2003

[16] Svantesson T., Ranheim A. Mutual coupling effects on the capacity of multielement antenna systems. Proceedings of IEEE international Conf. Acoustics, Speech, and Signal Processing, 2001, (2485-2488).

[17] Hui H.T. Practical dual-helical antenna array for diversity/MIMO receiving antennas on mobile handsets. IEEE Proceedings of Microwave, Antennas and Propagation 2005; 152 (5) 367-372.

[18] Pedersen G.F., Andersen J.B. Handset antennas for mobile communications: integration, diversity, and performance. Review of Science Radio 1996-1999, Wiley – IEEE Press 1999; 119-138.

[19] Kalliola K., Sulonen K., Laitinen H., Kivekas O., Krogerus J., Vainikainen P. Angular power distribution and mean effective gain of mobile antenna in different propagation environments. IEEE Trans. Vehicular Technology 2002; 52 (5) 823-838.

[20] Chiau C.C., Chen X., Parini C.Q. A compact four-element diversity antenna array for pda terminals in a MIMO system. Microwave and Optical Technology Let., 2005; 44 (5) 408- 412

[21] Ko S.C.K., Murch R.D. Compact integrated diversity antenna for wireless communications. IEEE Trans. Antennas and Propagation 2001; 49 (6) 954-960.

[22] Salonen I., Vainikainen P. Estimation of signal correlation in antenna arrays. Proceedings of 12th International Symp. on Antennas, Vol. 2, (383-386), Nov. 2002.

[23] Volakis J.L. Antenna engineering handbook. 4th Edition, Mc Graw Hill Companies, 2007.

[24] Turkmani A.M.D., Arowojolu A.A., Jefford P.A., Kellett C.J. An experimentation evaluation of the performance of two-branch space and polarization diversity schemes at 1800 MHz. IEEE Trans. Vehicular Technologies 1995; 44 (2) 318-326.

[25] Mallahzadeh A.R., Eshaghi S., Alipour A. Multiport characteristics of a wide-band cavity backed annular patch antenna for multipolarization operations. Progress in Electromagnetics Research 2009; 187-203.

[26] Chae S.H., Oh S.K., Park S.O. Analysis of mutual coupling, correlations, and TARC in Wibro MIMO array antenna. IEEE Antennas and Wireless Propagation Let. 2007; 6 122-125.

[27] P.Thongbor, A.Ruengwaree* and V.Pirajnanchai , “Rectangular Monopole Antenna with Arrow-Shaped Slot Etching for UWB-MIMO Application ” Conference Paper · June 2016.

[28] AISSAOUI Abderrahmane, REBAI Walid, “Effect of Concavity and Slots on Rectangular Patch Antennas” Master Project. IEEE/ University M’Hamed BOUGARA, Boumerdes, 2019.

Appendix

CST MICROWAVE STUDIO

To refine the calculated results, we have used the COMPUTER SIMULATION TECHNLOGY MICROWAVE STUDIO (CST MWS) software instead of the IE3D software for [31]. CST is a 3D simulator that is based upon a Finite Integration Technique (FIT) very similar to the finite different time domain (FDTD) analysis one. Whereas IE3D is based on MoM solution which is not suitable for large antenna array application. Thus, for simpler shape like rectangular or circular, a slight difference in results may be obtained due to the difference in the methods of analysis and the algorithm of the EM simulation software, which is the case for us.

CST MWS is an efficient tool for 3D EM simulation enabling high accuracy simulation results for complex antenna structures and it specifically suitable for wideband antenna simulation. It has a much better interface which enables the user to include very fine details in the geometry of the simulated structure. This software offers a number of different solvers, mainly time and frequency domain for its high accuracy, and that's for a different types of application in a very high frequency range.

CST is generally used in different type of antenna simulations, where all the parameters can be obtained like the S-parameters, input impedance, current distribution, VSWR, radiation patterns at all the planes as well as many other features that were very helpful during our simulations.

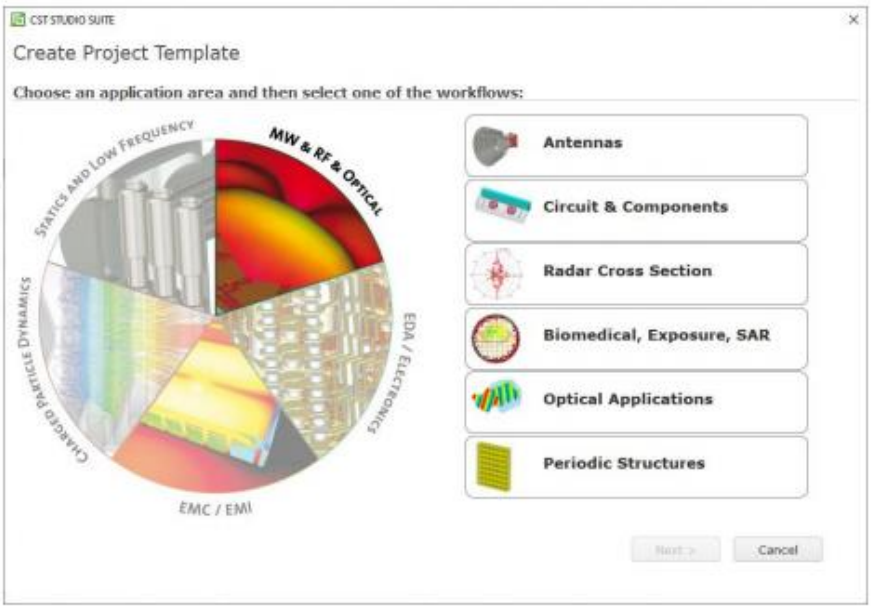

Figure A.1 shows the different application the in CST software.